Oxidative respiration through the *bd*-I and *cbb*$_3$ oxidases is required for *Vibrio cholerae* pathogenicity and proliferation *in vivo*.

Van Alst, Andrew. J.[1], Demey, Lucas M.[1], and DiRita, Victor J.[1*]

[1]Department of Microbiology and Molecular Genetics, Michigan State University, East Lansing MI 48824, USA

* Corresponding author

E-mail: diritavi@msu.edu

Author Contributions

Conceptualization, A.J.V and V.J.D.; Methodology, A.J.V. and V.J.D.; Validation A.J.V.; Formal Analysis A.J.V.; Investigation A.J.V. and L.M.D; Resources, V.J.D.; Writing – Original Draft, A.J.V.; Writing – Review & Editing, A.J.V. and V.J.D.; Visualization, A.J.V.; Funding Acquisition, V.J.D.

Data Availability

The authors confirm that all data underlying the findings of this work are fully available without restriction.

Abstract

Vibrio cholerae respires both aerobically and anaerobically and, while oxygen may be available to it during infection, other terminal electron acceptors are proposed for population expansion during infection. Unlike gastrointestinal pathogens that stimulate significant inflammation leading to elevated levels of oxygen or alternative terminal electron acceptors, *V. cholerae* infections are not understood to induce a notable inflammatory response. To ascertain the respiration requirements of *V. cholerae* during infection, we used Multiplex Genome Editing by Natural Transformation (MuGENT) to create *V. cholerae* strains lacking aerobic or anaerobic respiration. *V. cholerae* strains lacking aerobic respiration were attenuated in infant mice 10^5-fold relative to wild type, while strains lacking anaerobic respiration had no colonization defect, contrary to earlier work suggesting a role for anaerobic respiration during infection. Using several approaches, including one we developed for this work termed Comparative Multiplex PCR Amplicon Sequencing (CoMPAS), we determined that the *bd*-I and cbb_3 oxidases are essential for small intestinal colonization of *V. cholerae* in the infant mouse. The *bd*-I oxidase was also determined as the primary oxidase during growth outside the host, making *V. cholerae* the only example of a Gram-negative bacterial pathogen in which a *bd*-type oxidase is the primary oxidase for energy acquisition inside and outside of a host.

Keywords: *Vibrio cholerae*, respiration, oxygen, oxidase, pathogen, metabolism

Author Summary

The bacterium that causes cholera, *Vibrio cholerae*, can grow with or without oxygen. When growing without oxygen it may use other molecules that serve the same purpose as oxygen, acting as a terminal electron acceptor in an energy-generating process known as respiration. Given the largely anaerobic nature of the gastrointestinal tract, and the lack of significant inflammation during cholera infection, a process that can stimulate elevated levels of oxygen and other terminal electron acceptors, we sought to understand the respiratory mechanisms of *V. cholerae* during infection. We used a powerful genome-editing method to construct mutant strains of *V. cholerae* lacking some or all of the complement of proteins required for aerobic or anaerobic respiration. By analyzing these mutants in the laboratory and in intestinal colonization of infant mice, we determined that the ability to respire without oxygen is completely dispensable for *V. cholerae* to thrive during infection. We determined that two of the four oxygen-dependent respiration mechanisms are essential for *V. cholerae* to grow during infection, with the other two dispensable for wild type levels of colonization.

Introduction

Respiration promotes growth and proliferation of bacterial cells [1]. Energy acquisition through respiration relies on the metabolism of exogenously acquired substrates and the presence of terminal electron acceptor molecules to generate chemical energy, which is stored in the form of ATP to power cellular processes required for growth. Although not considered canonical virulence factors, metabolism and energy generative processes are required by pathogens to thrive during infection. Here we investigate respiration as a potent driver of replication during infection by the bacterial gastrointestinal pathogen *Vibrio cholerae* [2].

Vibrio cholerae is a facultative anaerobe that grows in both aerobic and anaerobic environments [3]. Respiration in *V. cholerae* is achieved aerobically through the terminal reduction of molecular oxygen or anaerobically through the terminal reduction of various alternative electron acceptors [4,5]. Recent evidence suggests there is combined contribution of both aerobic and anaerobic metabolism to *V. cholerae* growth *in vivo* [6,7]. This may be attributed to the radial and longitudinal gradients of oxygen availability in the intestinal tract enabling metabolism through both pathways in response to *in vivo* localization [8].

We sought to investigate the relative contributions of aerobic and anaerobic respiration *in vivo* using an infant mouse model of colonization. *V. cholerae* encodes four terminal oxidases and four terminal reductases that support respiration [9,10]. The terminal oxidases include one cbb_3 heme-copper oxidase [11,12] and three *bd*-type oxidase complexes capable of catalyzing the 4 H^+/O_2 reduction of oxygen to water [13]. cbb_3 oxidases [14,15] and *bd* oxidases [16–18] have a low K_m for oxygen and are typically induced under microaerobiosis, a feature particularly beneficial for pathogens colonizing near hypoxic environments of the human host [19–21]. *V. cholerae* also carries out anaerobic respiration through four terminal reductases that use either nitrate, fumarate, trimethylamine-N-oxide (TMAO) or biotin sulfoxide (BSO) [5,10,22,23]. Previous work found that abrogation of nitrate reductase activity reduced colonization in a streptomycin-treated adult mouse by approximately 2-fold [4] and a concomitant disruption in fermentative pathways further reduced colonization, revealing a dependency between nitrate reduction and fermentation [7]. Additionally, TMAO influences virulence gene expression in *V. cholerae* when added exogenously, however, whether reduction of TMAO is required for this response is not clear [5,24]. In this study, we looked to more thoroughly examine the complete suite of terminal electron accepting complexes encoded by *V. cholerae* and assess the pertinence of each terminal electron acceptor molecule to *in vivo* infection.

By targeting terminal oxidase and terminal reductase complexes of *V. cholerae*, we can better understand the respiratory processes occurring during disease and identify which terminal electron accepting complexes are most critical to *in vivo* fitness. This work highlights that oxygen, although present at low levels diffusing from the host epithelium, is sufficient and essential to supporting *V. cholerae* growth in the infant mouse. These findings change how we understand the host environment during *V. cholerae* pathogenesis and how oxygen may function in the pathogenicity of other bacterial pathogen elicited diseases.

Results

Constructing Terminal Electron Acceptor Mutant Strains

Vibrio cholerae terminal electron acceptor mutants were generated using the multiplex genome editing technique MuGENT [25] and by positive allelic exchange vector pKAS32 [26] in an El Tor C6706 *V. cholerae* background. Target loci and their relative chromosomal locations are depicted in Fig 1A. In MuGENT-generated mutant strains, target loci are disrupted by a frameshift mutation, removal of ATG start codon, insertion of 3-frame stop codons, and offseting of the ribosomal binding site. This is combined with the insertion of a universal detection sequence at each target locus and a spectinomycin cassette insert into pseudogene VC1807 for naturally competent cell selection that has no *in vitro* fitness cost [27] (S1 Fig.). MuGENT generated strains are designated with a superscript 'Mu' (^{Mu}). Mutant strains constructed via pKAS32 have the complete coding sequence for all subunits of target terminal electron acceptor complexes excised, generating isogenic deletion strains. Select strains were verified by whole genome sequencing which indicated no nucleotide polymorphisms in most strains and where present were found in hypothetical protein regions of the genome predicted to have no impact on bacterial cell fitness (S1 Table).

Fig 1. Verification of MuGENT generated mutant strains.

(a) Chromosomal map of *V. cholerae* terminal electron reducing complex loci. (b) Multiplex allele-specific PCR (MASC-PCR) of *V. cholerae* terminal electron reducing complexes MuGENT mutants. Lanes are labelled with the strain name where a strain preceded by a '^{Mu}+' (Lanes 3-6) indicates the oxidase complex as the sole remaining functional oxidase in that strain and strains preceded by a '^{Mu}' (Lanes 7-10) indicates that the specified locus is the targeted knock out. Targeted gene loci are labelled to the right of each gel image. The presence of a band indicates a targeted knockout in the gene locus whereas the absence of a band indicates the wild type gene is present.

V. cholerae encodes one *cbb*$_3$ oxidase and three *bd*-type oxidase complexes [9]. Cytochrome oxidase *cbb*$_3$ is a four subunit (VC1439-VC1442) cytochrome c containing terminal oxidase of which the coding sequence for the primary subunit, CcoN (VC1442), was disrupted to generate MuGENT knockout strains. CcoN is the first open reading frame in the operon and contains the active site for reducing oxygen to water [28]; its disruption was sufficient for abolishing *cbb*$_3$ cytochrome c activity (S2A Fig). For each of the three *bd*-type oxidases, *bd*-I (VC1844-43), *bd*-II (VCA0872-73), and *bd*-III (VC1570-71), both subunits of each complex were disrupted. Mutations in each target locus were confirmed by multiplex allele-specific PCR (MASC-PCR) [29] where the presence of a DNA band indicates successful genomic editing at the indicated locus via MuGENT (Fig 1B). To further validate the function of each oxidase, isogenic deletion strains were also generated for select terminal oxidases via pKAS32 positive allelic exchange.

V. cholerae also encodes four alternative terminal reductase complexes [9] capable of reducing alternative electron acceptors that can support respiration in the absence of oxygen. The four terminal reductases include a fumarate reductase (VC2656-59), trimethylamine-N-

oxide (TMAO) reductase (VC1692-94), nitrate reductase (VCA0676-0680), and a biotin sulfoxide reductase (BSO) (VC1950-51). For each of these multi-subunit complexes, the active reducing subunit was disrupted via MuGENT and confirmed by MASC-PCR (Fig 1B).

In vitro Characterization of Terminal Electron Acceptor Complex Mutants

Terminal Oxidase Growth Characterization

V. cholerae oxidase mutant strains were grown in LB media in aerobic and anaerobic conditions. Inocula were prepared anaerobically to ensure consistent growth of oxidase-deficient strains. After anaerobic preparation of inocula, both *cbb*$_3$ and *bd*-I oxidase complexes were found to be required for wild type levels of growth in aerobic conditions whereas *bd*-II and *bd*-III oxidases were not (Fig 2A). Cultures lacking the *cbb*$_3$ oxidase grew at a consistently lower optical density and never reached the peak OD_{600} of wild type. The *bd*-I oxidase was determined to be the most critical oxidase complex for supporting aerobic respiration in *V. cholerae*, as cells lacking it showed drastically reduced growth. This finding was unexpected as electron transport and oxygen reduction by the *cbb*$_3$ oxidase is more efficient at generating a proton gradient (and therefore ATP) for the cell [30]. Electrons passed to the *cbb*$_3$ oxidase are shuttled through the cytochrome bc_1 complex, which accounts for a $\Delta 6H^+$ proton gradient [31] along with translocation of two additional protons coupled to the terminal reduction of oxygen by the *cbb*$_3$ complex [32]. The *bd*-I reducing pathway, as with all *bd*-type oxidases, generates a relatively weaker proton gradient resulting in less ATP for the cell [13,33]. Thus our observation that it serves as the primary oxidase in *V. cholerae* under atmospheric oxygen conditions was unanticipated. All oxidase-disrupted mutants grew comparably to wild type in anaerobic conditions (Fig 2B) suggesting the observed defect in aerobic growth is not due to a general

171 growth defect imposed by the mutations. *In vitro* competition assays were also performed,
172 demonstrating a competitive defect for both *cbb*$_3$ and *bd*-I deficient strains in aerobic conditions
173 (Figs 2C and 2D). These growth phenotypes were recapitulated in M9 0.2% D-glucose media,
174 although *bd*-I deficient strains were further hampered for growth aerobically and showed a minor
175 shift in reaching exponential phase anaerobically (S3A and S3B Figs).
176
177 **Fig 2. Terminal oxidases support aerobic growth in *V. cholerae*.**
178 Growth characteristics of the terminal oxidases in *V. cholerae.* (a-b) Single terminal oxidase
179 mutants, both MuGENT and isogenic deletion, growth in LB. Inoculums were prepared
180 anaerobically and subsequently grown in aerobic and anaerobic conditions, respectively. (c-d)
181 Single terminal oxidase isogenic deletion strain *in vitro* LB competition assays in both aerobic
182 and anaerobic conditions, respectively. Competitive index scores were calculated as a ratio of
183 output versus input [(Target$_{Output}$/*ΔlacZ*$_{Output}$) / (Target$_{Input}$/*ΔlacZ*$_{Input}$)], where a *ΔlacZ* strain served
184 as a psuedo-wild type to determine relative fitness via blue-white screening. Red dots indicate
185 the limit of detection where no target strain CFUs were recovered for these trials. (e-f) Single
186 terminal oxidase isogenic deletion mutant growth in LB where inoculums were prepared
187 aerobically and subsequently grown in aerobic and anaerobic conditions, respectively. (g) *In*
188 *vitro* expression of terminal oxidases in anaerobic, microaerobic, and aerobic growth conditions.
189
190 We hypothesized that *bd*-I deficient strains grown anaerobically may experience a
191 growth lag prior to expression of alternative oxidases, such as the *cbb*$_3$ oxidase (S2B Fig),
192 accounting for the observed growth kinetics. To test this, we prepared inocula aerobically and
193 observed the growth phenotype. In this condition, strains lacking *bd*-I oxidase grew to wild type
194 optical density (Fig 2E) indicating that delayed expression of alternative oxidases when inocula
195 are prepared anaerobically may account for the observed growth lag. Similar growth patterns
196 were observed among all strains in anaerobic growth conditions for inocula of aerobically

197 prepared oxidase mutants (Fig 2F). We examined expression patterns of wild type *V. cholerae*
198 under anaerobic, microaerobic, and aerobic conditions and determined relative quantification of
199 gene expression by an elongated Pfaffl method detailed in Materials and Methods. *recA* served
200 as the gene of reference and expression values are reported relative to *bd*-III expression in
201 anaerobic conditions which served as the comparator target for relative expression among the
202 oxidases (Fig 2G). The cbb_3 and *bd*-I oxidases were highly expressed relative to *bd*-II and *bd*-III.
203 In anaerobic conditions, the *bd*-I oxidase was expressed nearly 10-times higher than the cbb_3
204 oxidase, whereas in the presence of oxygen (microbaerobic or aerobic), *bd*-I oxidase was
205 expressed only marginally higher than cbb_3 oxidase. We conclude from the growth assays and
206 expression profiles that the *bd*-I oxidase is critical for aerobic respiration in *V. cholerae* during
207 transition from an anaerobic to aerobic environment and hypothesize that expression of the cbb_3
208 oxidase is delayed during this transition period.
209
210 Further characterization of the oxidase complexes was carried out using double, triple,
211 and quadruple oxidase mutant strains. Isogenic double and triple deletion strains, as well as
212 quadruple oxidase MuGENT mutant Aero7, were grown in aerobic and anaerobic conditions in
213 LB from inocula grown anaerobically (Figs 3A and 3B). Strain +*bd*-I, harboring solely a
214 functional *bd*-I oxidase, grew to near wild type levels while strains +cbb_3 and +*bd*-III, having
215 solely the cbb_3 or *bd*-III oxidase complex, grew after a considerable lag phase. This lag phase,
216 however, was reduced when inocula were adapted to an aerobic environment prior to the
217 growth assay (Figs 3C and 3D). Growth phenotypes were comparable to triple oxidase
218 MuGENT strains, although strain ^{Mu}+*bd*-III (encoding only *bd*-III) exited lag phase more rapidly
219 (S3C and S3D Figs). Strain Aero7, defective for production of all terminal oxidases encoded by
220 *V. cholerae*, and strain +*bd*-II, containing only the *bd*-II oxidase, were completely deficient for
221 aerobic growth. This was further exemplified for Aero7 by a near 10^7-fold attenuation in *in vitro*
222 competition assays (Fig 3E). From these results, we conclude that cbb_3, *bd*-I, and *bd*-III

223 oxidases support aerobic growth of *V. cholerae* to varying degrees while *bd*-II does not. Despite
224 its low mRNA expression level in wild type cells relative to other oxidases, *bd*-III oxidase
225 supported +*bd*-III aerobic growth, particularly when culture inocula were grown aerobically.
226
227 **Fig 3. Individually, oxidases *cbb*$_3$, *bd*-I, and *bd*-III support aerobic growth in *V. cholerae*.**
228 (a-b) Combinatorial terminal oxidase deletion mutant growth in LB. Inoculums were prepared
229 anaerobically and subsequently grown in aerobic and anaerobic conditions, respectively. Triple
230 deletion mutant strains have a '+' with an oxidase name (e.g. +*cbb*$_3$), indicating the sole
231 remaining oxidase, with the other three oxidases disrupted by mutation. (c-d) Combinatorial
232 terminal oxidase deletion mutant growth in LB. Inoculums were prepared aerobically and
233 subsequently grown in aerobic and anaerobic conditions, respectively. (e) *In vitro* aerobic and
234 anaerobic competition assay between Aero7 and wild type *V. cholerae* with competitive index
235 scores calculated as [(Aero7$_{Output}$/WT$_{Output}$) / (Aero7$_{Input}$/WT$_{Input}$)]. Growth curves are an average
236 of three biological replicates where error bars represent the standard error of the mean. Bars for
237 *in vitro* competitions and expression data represent the arithmetic mean where error bars
238 represent the standard error of the mean.
239
240 Taken together, these findings make clear that *bd*-I oxidase is the primary oxidase in *V.*
241 *cholerae*, priming a transition from anaerobic to aerobic environments and functioning as the
242 primary oxidase in atmospheric oxygen environments. To our knowledge, *V. cholerae* and
243 *Listeria monocytogenes* [34] are the only pathogens demonstrated to preferentially use a *bd*-
244 type oxidase in lieu of a heme-copper oxidase such as the *bo*$_3$ oxidase of *Escherichia coli* [35]
245 and *Salmonella* Typhimurium [36], the *cbb*$_3$ oxidase of *Psuedomonas aeruginosa* [37],
246 *Campylobacter jejuni, and Helicobacter pylori* [38], or the *aa*$_3$ oxidase of *Staphylococcus aureus*
247 [39] to support growth in atmospheric oxygen.
248

Growth of Mutants Lacking Terminal Reductases

MuGENT terminal reductase *V. cholerae* mutants were prepared aerobically and used to inoculate fresh LB with and without alternative electron acceptors in both aerobic and anaerobic conditions. Individual reductase MuGENT-derived mutant strains were made lacking the active subunit of fumarate reductase (VC2656), TMAO reductase (VC1692), nitrate reductase (VCA0678), and BSO reductase (VC1950). A combinatorial mutant was also constructed, denoted Ana4, in which all reductases were disrupted.

All terminal reductase mutants, including Ana4, grew similarly to wild type in LB in both aerobic and anaerobic growth conditions. However, when grown anaerobically in the presence of the alternative electron acceptors fumarate, TMAO, nitrate, or DMSO, mutant strains were defective for growth compared to wild type (Figs 4A-4D). This indicated that the MuGENT-generated reductase mutants were defective for reductase function. As Ana4 was reduced for growth in the presence of all alternative electron acceptors, we concluded it adequately represented a strain incapable of utlizing these molecules to support growth via anaerobic respiration and included it in our *in vivo* analysis described below. The presence of these alternative electron acceptors under aerobic conditions led to varying growth responses by wild type *V. cholerae*. With fumarate or DMSO, growth was boosted, however, with either nitrate or TMAO growth was reduced (S4A-S4D Figs).

Fig 4. Terminal reductase mutants are reduced for anaerobic growth in the presence of cognate electron acceptor molecules.

Growth characteristics of terminal reductases of *V. cholerae*. MuGENT generated terminal reductase mutants grown in LB in the presence and absence of alternative electron acceptors (a) 50mM fumarate, (b) 50mM trimethylamine-N-oxide (TMAO), (c) 50mM nitrate, and (d) 50mM

dimethyl sulfoxide (DMSO). Inoculums were prepared aerobically and subsequently grown in anaerobic conditions. Growth curves are an average of three biological replicates where error bars represent the standard error of the mean.

Aero7 and Ana4 Infant Mouse Infections

To examine the importance of aerobic and anaerobic respiration during infection, *V. cholerae* Aero7 and Ana4 MuGENT strains were tested for their ability to colonize the infant mouse intestinal tract. Single strain and competition infections in neonatal mice were performed for both strains.

Aero7 was severely attenuated for colonization of the small intestine, in both single strain and competition infections (Figs 5A and 5B). In single strain infections, wild type *V. cholerae* was recovered near 10^8 CFU/g intestine whereas Aero7 was recovered near 10^3 CFU/g intestine, a 5-log decrease in colonization. This reduction was also observed in the competition infections where the competitive index (CI) score of Aero7, calculated as $[[Aero7_{Output}/WT_{Output}] / [Aero7_{Input}/WT_{Input}]]$ was approximately 10^{-5}. Aero7 competed better in the large intestine, although was still at a fitness disadvantage, with a CI of 10^{-3}. Its greater fitness in the large intestine may be due to the more anaerobic environment of this site (S5A and S5B Figs). That Aero7 is considerably less fit in the infant mouse small intestine is relevant as this is the site of infection in humans. We conclude from these findings that maintaining functional terminal oxidases, and therefore aerobic respiration, is critical for *V. cholerae* to establish infection and proliferate.

Fig 5. Aerobic respiration, but not anaerobic respiration, is required for growth and colonization of the infant mouse small intestine.

299 Aero7 and Ana4 small intestine colonization in single strain and competition infections. (a)
300 Single strain infection of strain Aero7. (b) Competition infection of strain Aero7. (c) Single strain
301 infection of strain Ana4. (d) Competition infection of strain Ana4. Bars represent the geometric
302 mean. Horizontal dashed lines indicate the limit of detection (LOD) and red dots indicate
303 recovered CFUs were below the LOD. Competitive index scores were calculated as
304 $[(Mutant_{Output}/WT_{Output}) / (Mutant_{Input}/WT_{Input})]$. Statistical analysis was performed using GraphPad
305 PRISM. *, $P < 0.05$. A Mann-Whitney U-test was used in the determination of significance
306 between WT and Aero7. A Student's *t* test was performed on log transformed data in the
307 determination of significance between WT and Ana4.
308
309 In contrast to a strain lacking all terminal oxidases, the Ana4 mutant lacking all terminal
310 reductases, which is deficient for growth via anaerobic respiration (Figs 4A-4D), colonized both
311 the small and large intestines to wild type levels in both single strain and competition infections
312 (Figs 5C and 5D and S5C and S5D Figs). The lack of an observable phenotype in our
313 experiments differs from an earlier study demonstrating a two-fold reduction in colonization by a
314 mutant strain of *V. cholerae* lacking nitrate reductase (*napA*; VCA0678) in the adult
315 streptomycin-treated mouse model [4]. This two-fold reduction may be observed in adult mice,
316 but not infant, as the adult gut has greater anaerobic luminal volume compared to the limited
317 luminal space in the infant. Alternatively, nitrate availability has also been shown to increase
318 following streptomycin treatment, which may contribute to the observed colonization
319 discrepancy between wild type and *napA V. cholerae* [40], as lacking a functional nitrate
320 reductase may incur a greater fitness cost in the streptomycin-treated adult mouse.
321
322 Overall, our data suggests that anaerobic respiration using alternative electron acceptors
323 is not a prominent feature of *V. cholerae* growth during infection of the infant mouse. The slight
324 growth defect reported with a nitrate reductase mutant in the streptomycin-treated adult mouse

[4] suggests that there may be a limited role for anaerobic respiration although more work is required to ascertain the effects of a mature, non-disturbed microbiota on these questions.

Individual Oxidase Function During Infection

Comparative Multiplex PCR Amplicon Sequencing (CoMPAS)

To examine the requirements of the terminal oxidases of *V. cholerae in vivo*, we took a novel approach that combines elements of insertion-site sequencing (Tn-Seq) with targeted amplification of MuGENT generated oxidase mutations (Comparative Multiplex PCR Amplicon Sequencing (CoMPAS)). Individual terminal oxidase MuGENT strains were pooled along with a wild type strain in equal proportions, and served as the inoculum to infect infant mice. The small intestines were pooled from 6 mice and genomic DNA extracted along with the input inoculum for CoMPAS analysis.

Mutant allele abundances were determined for each oxidase complex and relative sequence abundances were normalized to *toxT* gene amplification (Fig 6A). Sequence coverage for each pool are presented in S2 Table. Comparative index scores are reported for each of the primary oxidase subunits VC1442 (cbb_3), VC1844 (*bd*-I), VCA0872 (*bd*-II), and VC1571 (*bd*-III). Comparative index scores were calculated as [(Output $Pool_{Target\ Reads}$ / Output $Pool_{toxT\ Reads}$) / (Input $Pool_{Target\ Reads}$ / Input $Pool_{toxT\ Reads}$)]. In this experiment, ^{Mu}*bd*-I oxidase knockout strain was underrepresented in the output sequencing pool approximately 10-fold relative to the input. Conversely, all other MuGENT oxidase mutant strains were within a 2-fold change relative to the input. Overall, the *bd*-I oxidase was at a competitive disadvantage in the pooled infection and was determined to be the most important oxidase complex supporting growth *in vivo*.

Fig 6. *bd*-I oxidase is critical in competitive infection of the infant mouse small intestine, yet colonization is supported by functional redundancy of terminal oxidases in single strain infections.

Single oxidase *in vivo* colonization dynamics in the small intestine. (a) Comparative Multiplex PCR Amplification Sequencing (CoMPAS) sequence analysis. Comparative index scores were calculated as [(Output $Pool_{Target\ Reads}$ / Output $Pool_{\textit{toxT}\ Reads}$) / (Input $Pool_{Target\ Reads}$ / Input $Pool_{\textit{toxT}\ Reads}$)]. Vertical red dashed lines indicate a 2-fold change in output to input sequence ratios. Sequence coverage for each input pool (IP) and associated mouse output pool (MP) are shown in the bar plots. (b) Individual oxidase deletion single strain infections. Bars represent the geometric mean. Horizontal dashed lines indicate the limit of detection (LOD) and red dots indicate recovered CFUs were below the LOD. Statistical analysis was performed using GraphPad PRISM. *, $P < 0.05$. A Mann-Whitney U-test was used in the determination of significance between WT and Aero7 whereas an Analysis of Variance with *post hoc* Dunnett's multiple comparisons test was conducted on log transformed CFU/g intestine for all other strain comparisons.

Single Oxidase Complex Deletion Infections

Isogenic terminal oxidase deletion strains were also examined for colonization levels in single strain infections of the infant mouse. Loss of any one of the terminal oxidases did not result in a colonization defect in the small or large intestine of the infant mouse (Fig 6B and S5E Fig). Wild type and mutant strains colonized to approximately 10^8 CFU/g intestine. Counter to the observed defect in a ^{Mu}*bd*-I knockout strain in our CoMPAS analysis, no colonization defect was present in single strain infections. These findings indicate that in single strain infections, loss of the *bd*-I oxidase was not detrimental to colonization and that likely functional redundancy exists among the oxidases that can support aerobic respiration during noncompetitive infection.

We reasoned that a *bd*-I oxidase deficient strain was capable of colonizing the infant mouse, however, as cultures prepared anaerobically were delayed for aerobic growth as in Fig 2A, this growth delay resulted in the *bd*-I deficient strain being outcompeted during the pooled mouse infection. As multiple oxidases were shown to support aerobic growth of *V. cholerae* in our growth assays, we hypothesized that the cbb_3, *bd*-I, and potentially the *bd*-III oxidase could all be supporting growth *in vivo*. This hypothesis also reflects data present in a large Tn-Seq dataset where transposon insertions into the cbb_3, *bd*-I, and *bd*-III oxidases showed a reduced capacity for colonization [41].

For all oxidase mutants, one concern is that disruption to oxidase function may impact other requirements for colonization such as virulence factor production or protection against reactive oxygen species (ROS). To determine whether mutations in the oxidases alter production of virulence factors required for colonization, TcpA protein levels in the mutants were examined as described in Supplemental Materials and Methods and were equivalent to wild type production (S6A-S6C Figs). As oxidative stress can also prevent bacterial growth *in vivo* and the *bd* oxidases of *Escherichia coli* exhibit low levels of catalase activity [42], we tested the minimum inhibitory concentraion of hydrogen peroxide on *V. cholerae* oxidase mutants, observing no growth defects for any mutant strain (S6D Fig). These findings support our conclusions that observed colonization defects can be attributed to a reduction in respiratory energy generation and not related to virulence factor production or increased ROS sensitivity that could have also limited colonization efficiency.

Determining Functionally Redundant Oxidases During Infection

To identify which oxidases primarily support growth *in vivo*, triple oxidase isogenic deletion strains were used to colonize the infant mouse. By infecting with triple mutants, we could determine the importance of the single remaining oxidase. Strain +*bd*-I expressing solely the *bd*-I oxidase colonized comparable to wild type and strain +cbb_3 with a functional cbb_3 oxidase colonized at a ~1.5-fold reduction compared to wild type (Fig 7A). This finding further supports *bd*-I oxidase as the primary oxidase of *V. cholerae*. Strains containing solely the *bd*-II or *bd*-III oxidase were unable to colonize (Fig 7A). This pattern of colonization was also reflected in the large intestine, however with higher levels of recovered CFU/g intestine, again likely due to the more anaerobic environment (S5F Fig). As the cbb_3 oxidase was determined to be less expressed and inactive in anaerobic conditions (Fig 2G and S2B Fig), and mouse inocula were prepared anaerobically prior to infection, we investigated whether preparation in aerobic conditions could prime expression and activation of the cbb_3 oxidase to better support growth *in vivo*. However, despite preparing +cbb_3 oxidase cultures aerobically, we still observed a significant ~1-log reduction in colonization (Fig 7B). The colonization efficiency of aerobically grown +cbb_3 cultures was improved compared to anaerobically prepared +cbb_3 cultures but was not enough to support wild type levels of colonization. No significant difference was detected in the large intestine, which was also previously observed in the anaerobically prepared culture infections (S5G Fig).

Fig 7. *bd*-I oxidase alone supports wild type levels of colonization in the infant mouse small intestine with cbb_3 supporting colonization to a lesser extent.

(a) Combinatorial oxidase deletion i*n vivo* colonization dynamics in the small intestine. (b) Colonization of aerobically prepared wild type and +cbb_3 oxidase inoculums in the small

intestine. Triple deletion mutant strains have a '+' with an oxidase name (e.g. +*cbb*$_3$), indicating the sole remaining oxidase, with the other three oxidases disrupted by mutation. Bars represent the geometric mean. Horizontal dashed lines indicate the limit of detection (LOD) and red dots indicate recovered CFUs were below the LOD. Statistical analysis was performed using GraphPad PRISM. *, $P < 0.05$. A Mann-Whitney U-test was used in the determination of significance between WT and +*bd*-II, +*bd*-III, and Δ*cbb*$_3$Δ*bd*-I whereas an Analysis of Variance with *post hoc* Dunnett's multiple comparisons test was conducted on log transformed CFU/g intestine for all other strain comparisons. *, $P < 0.05$.

As the +*bd*-III oxidase strain grew *in vitro* in aerobic LB conditions following aerobic overnight preparation while lacking both *cbb*$_3$ and *bd*-I oxidases, we looked to determine whether wild type expression levels of *bd*-III oxidase could support aerobic growth in this strain. By relative quantification of gene expression using an elongated Pfaffl method, +*bd*-III aerobic growth was found to be supported by increased expression of *bd*-III transcript, minimally 80x higher than wild type (S7A Fig). We hypothesized that this increased expression may be due to selective pressure for mutations that increase *bd*-III expression. A variant strain, +*bd*-III^{V} was isolated that supported high levels of aerobic growth, had no defect for anaerobic growth, and exhibited increased expression of the *bd*-III oxidase (S7B-S7D Figs). We determined the genome sequence of this variant, identifying a mutation in *chrR* (VC2301), encoding an anti-sigma factor for SigmaE, which controls *bd*-III expression (S1 Table) [43]. In infant mouse infections, +*bd*-III^{V} colonized near one order of magnitude lower than wild type in the small intestine of the infant mouse and was comparable to wild type in the large intestine (S7E and S7F Figs). Comparatively in infant mouse infections, the +*bd*-III^{V} strain performed significantly better than +*bd*-III in the initial colonization infections (Fig 7A). In wild type *V.* cholerae, we found that the *bd*-III oxidase is not typically expressed and does not contribute to *in vivo*

colonization, however, in scenarios where the *bd*-III oxidase is the sole remaining oxidase and is expressed, it can support aerobic growth and *in vivo* colonization.

Discussion

Terminal oxidases *cbb*$_3$, and particularly *bd*-I, serve as the major terminal reducing complexes to support the oxidative respiration required for population expansion of *V. cholerae* in the infant mouse. This is the first instance where a *bd*-type oxidase was determined to be the primary oxidase supporting growth of a Gram-negative bacterial pathogen in both atmospheric and *in vivo* oxygen environments. In *V. cholerae*, the *bd*-I oxidase facilitated aerobic growth and was critical for a rapid shift to aerobic respiration metabolism when transitioning from an anaerobic to aerobic environment. The finding that the *cbb*$_3$ and *bd*-I oxidases of *V. cholerae* are necessary for aerobic respiration in the low oxygen environment of the small intestine aligns with the typically low K_m observed for each of these oxidase classes [19–21,44–46]. Our findings highlight that the low oxygen level in the small intestine is sufficient and essential for *V. cholerae* growth and implicates oxygen as a key electron acceptor for bacterial pathogenesis in the gut.

Investigating oxygen availability *in vivo* over the course of infection is important for understanding oxygen dynamics that shape *V. cholerae* pathogenesis. In *V. cholerae* infant rabbit infection, signatures of aerobic metabolism were observed as TCA cycle gene expression was upregulated due to the presence of cholera toxin [47], indicating the cholera toxin may induce oxygen influx into the intestinal lumen. Gut microbial succession following *V. cholerae* infection also suggests conversion to a more oxygenated gut during the course of disease as facultative anaerobes predominate following human infection and display increased transcriptional abundance of the high-affinity *cbb*$_3$ oxidase during infection that became less

abundant in the recovery period [48]. However, the direct relationship between *V. cholerae* and its cholera toxin on luminal oxygen availability has yet to be explored. In newly emergent strains of *V. cholerae*, intestinal cell damage has been found to occur with elevated bacterial loads in both mouse and rabbit models compared to previous pandemic strains [49]. Emergent strains capable of eliciting and withstanding inflammatory conditions of the intestine may benefit from increased oxygen availability, supporting enhanced population expansion. The findings of these studies support the conclusions made from this work, however, direct measurement of oxygen concentrations over the time course of disease remains to be determined.

In addition to the essential role of oxygen in growth and proliferation of *V. cholerae*, oxygen also serves as a signaling molecule regulating virulence gene expression in differentially oxygenated environments. *V. cholerae* maintains thiol-based switch regulators AphB and OhrR along with a two-component sensor ArcAB that respond to the presence of oxygen. Cysteine disulfide linkages that form within AphB and OhrR in reducing environments, such as the more anaerobic gut lumen, may prime *V. cholerae* cells for attachment by upregulating expression of the toxin coregulated pilus [50]. ArcAB also responds to oxygen, although indirectly through the action of redox active quinone electron carriers [51]. ArcA is typically activated in anaerobic conditions, yet in an experimental setup that favored microaerobic conditions, ArcA was needed for optimal virulence gene expression in the Classical biotype [52]. However, the contribution of ArcA to El Tor *V. cholerae* colonization and pathogenicity has yet to be explored. It is not unlikely there may be different mechanisms of ArcA regulation between Classical and El Tor *V. cholerae*, as the Classical biotype is incapable of producing cholera toxin under anaerobiosis [53] whereas the El Tor biotype can produce cholera toxin anaerobically [6]. Oxygen sensing may also drive a chemotactic response in *V. cholerae* through aerotactic chemoreceptors Aer1 [54] and Aer2 [55], however this oxygen response pathway is unlikely to be required *in vivo* as non-chemotactic *V. cholerae* nevertheless colonize the infant mouse intestine [56].

Oxygen has also been shown to be needed for growth and pathogenicity of other gastrointestinal pathogens including *E. coli* [57], *S.* Typhimurium [36], *L. monocytogenes* [34], and *C. jejuni* [58]. Infection with these pathogens leads to epithelial damage and gastroenteritis, which correlates with increases in luminal oxygen availability [59]. This influx of oxygen in the case of *E. coli* and *S.* Typhimurium further drives proliferation of these pathogens, exacerbating disease. In contrast, cholera is not typically characterized as an inflammatory disease, lacking gross pathological damage on host tissue, although *V. cholerae* does induce inflammatory markers in murine bone marrow-derived macrophages [60]. A question that emerges from our work is whether *V. cholerae* has a mechanism for driving oxygen into the gut to enhance growth and proliferation as do other intestinal bacterial pathogens. Our observation that oxidative respiration is critical for pathogen growth in the absence of tissue invasion, inflammation, and intestinal destruction is a novel finding in bacterial pathogenicity, although whether other microbes that thrive on inflammation-induced electron acceptors can acquire oxygen during infection prior to when inflammation occurs is not clear.

Through this work, we determine that oxidative respiration is essential to the replicative fitness of *V. cholerae* during infection. Despite the overall low concentrations of oxygen within the intestinal space, replication of *V. cholerae* is supported almost entirely by oxidative respiration to colonize the infant mouse small intestine. As oxygen in the human intestine is modulated by interactions between the host tissue and commensal microbial populations [36], new disease models of *V. cholerae* infection would be beneficial to investigate gut oxygen perturbations during disease. To enable colonization, *V. cholerae* mouse models require either the naïve intestine of the neonate with its limited microbiota, or antibiotic treatment of the adult [61,62]. In both instances, oxygen levels are predicted to be elevated compared to steady-state physiological hypoxia in the mature adult intestine [63,64]. Oxygen availability in these models,

and likely in human infection, is therefore positively correlated to successful colonization of the intestine. Monitoring oxygen concentrations *in vivo* over the course of infection is challenging but may be important for understanding oxygen dynamics that shape *V. cholerae* pathogenesis.

Acknowledgements

A.J.V. was supported in part by the Eleanor L. Gilmore Endowed Excellence Award in the Department of Microbiology and Molecular Genetics at Michigan State University. This work was supported in part by the Rudolph Hugh Endowment (V.J.D.) at Michigan State University.

Declaration of Interests

The authors declare no competing interests.

Materials and Methods

Ethics Statement

All animal experiments in this study were conducted in accordance with all necessary regulations and requirements and was approved by the Institutional Animal Care and Use Committee at Michigan State University (PROTO201900421). Per the IACUC approved protocols, dam mice were euthanized by carbon dioxide inhalation and secondary cervical dislocation, and neonatal mice were euthanized by lethal dose of isoflurane and secondary cervical dislocation.

Bacterial Strains and Growth Conditions

Bacterial strains used in this study are listed in S3 Table. *Vibrio cholerae* El Tor C6706 was used as the wild type strain in this study and served as the strain background for all *V. cholerae* mutant derivatives. Strains were grown primarily on LB agar and used to inoculate 4ml LB media in preparation for subsequent assays. Antibiotics when required were in given concentrations: streptomycin (100µg/ml), spectinomycin (200µg/ml), and ampicillin (100µg/ml). Strains were grown at 37°C for all growth assays. Aerobic growth assays were performed at atmospheric oxygen concentrations whereas anaerobiosis for anaerobic growth was maintained using a Coy anaerobic chamber.

MuGENT Mutant Strain Construction

MuGENT generated mutant strains were constructed using Enhanced Multiplex Genome Editing by Natural Transformation [25]. Linear segments of *V. cholerae* genomic DNA were amplified using a primer with intentional base changes designed to introduce a frameshift mutation, removal of ATG start codon, insertion of 3-frame stop codons, and offsetting of the ribosomal binding site while also inserting a universal primer binding site. These fragments, along with a fragment containing an antibiotic resistance cassette in pseudogene VC1807 were transformed into a *V. cholerae ΔrecJΔxseA* pMMB-tfoX strain. Once all mutants were integrated into the genome of carrier strains, a more traditional MuGENT approach [27] was used to amplify ~2Kb arms of homology on either side of the mutated site in each carrier strain to introduce into wild type *V. cholerae* by natural transformation, which maintains functional *recJ* and *xseA*. Candidate colonies were screened via colony PCR for target loci in a multiplex PCR reaction and confirmed by screening purified genomic DNA of each isolate. Strains were serially passaged in LB media to cure the pMMB-tfoX plasmid, where cured strains became sensitive to

ampicillin 100µg/ml. Primers used to generate and confirm MuGENT mutant strains are listed in S4 Table.

Isogenic Deletion Mutant Strain Construction

To confirm the phenotypes associated with MuGENT generated strains, isogenic deletion strains were also constructed. Growth phenotypes of isogenic deletion strains largely phenocopied MuGENT generated strains, thus we anticipated no off-target effects as equivalent growth was observed between mutant strains generated by two distinct DNA editing techniques. Whole genome sequencing was also used to validate select mutant strain genomes (See Supplemental Material). Isogenic deletion strain constructs were generated using the positive allelic exchange vector pKAS32 [26]. Plasmid constructs were generated by first amplifying and purifying 1Kb DNA fragments upstream and downstream of target loci that contain homology base pairing to pKAS32. The pKAS32 vector was isolated from *E. coli* pKAS32 cultures using a QIAprep Spin Miniprep Kit (Qiagen) and restriction digested with SacI and XbaI. DNA fragments and digested pKAS32 backbone were combined using Gibson Assembly (New England Biolabs) and transformed into *E. coli* ET12567 *ΔdapA* diaminopimelic acid auxotroph mating strain. Newly formed pKAS32 constructs were sequenced and correct vectors conjugated into *V. cholerae*. *V. cholerae*-pKAS32 strains were outgrown in LB at 37°C 210rpm and subjected to >2500µg/ml streptomycin to select for strains that have excised the plasmid from its genome. Candidate mutant strains were screened by colony PCR and confirmed by screening purified genomic DNA. Primers to generate and confirm pKAS32 deletion strains are listed in S4 Table.

V. cholerae Terminal Oxidase Strain Growth Curves

Bacterial strains were grown either aerobically or anaerobically on LB streptomycin (100µg/ml) agar media and after 16-18h used to inoculate 4ml LB media. After 16h, bacterial

strains were concentrated to a 1.0 OD_{600}. 700µl LB media was inoculated 1:1000 (0.7µl) with the 1.0 OD_{600} resuspensions, vortexed, and aliquoted in triplicate 200µl volumes in a 96-well plate. Optical density was recorded every hour for the duration of the growth curve. Deoxygenated LB was used for anaerobic growth and benchtop LB used for aerobic growth.

V. cholerae Terminal Reductase Strain Growth Curves

Bacterial strains were grown on LB streptomycin (100µg/ml) agar media and after 16-18h used to inoculate 4ml LB media. After 16h, bacterial strains were concentrated to a 1.0 OD_{600}. 700µl LB media was inoculated 1:1000 (0.7µl) with the 1.0 OD_{600} resuspensions, vortexed, and aliquoted in triplicate 200µl volumes in a 96-well plate. Optical density was recorded every hour for the duration of the growth curve. Deoxygenated LB was used for anaerobic growth curves and benchtop LB used for aerobic growth curves. Concentrations of alternative electron acceptors supplemented to LB media were as follows: 50mM sodium fumarate (Sigma), 50mM trimethylamine-N-oxide (TMAO) (Sigma), 50mM sodium nitrate (Sigma), and 50mM dimethyl sulfoxide (DMSO) (Sigma). For strains grown in 50mM LB Nitrate media, after 3h, 5µM sodium hydroxide (Fisher Chemical) final concentration was added to alkalinize the growth media to support continued nitrate respiration.

Wild Type Aerobic, Microaerobic, and Anaerobic RNA Isolation and Real-Time Quantitative PCR (RT-qPCR)

For each growth condition (aerobic / microaerobic / anaerobic) 4ml of LB media was placed in each environment at 37°C to temper the media prior to inoculation in an effort to equalize the oxygen content and to pre-warm the media. Media was inoculated 1:1000 (4µl) with a 1.0 OD_{600} wild type *V. cholerae* inoculum and grew shaking 210rpm for the aerobic culture and

618 static for both microaerobic and anaerobic cultures. After 4h, culture tubes were centrifuged
619 4000rpm, 4°C, for 10min and cell pellets were resuspended in 1ml TRIzol (Invitrogen). RNA was
620 isolated from TRIzol suspensions using an RNeasy kit (Qiagen) coupled with an on-column
621 DNase digestion (Qiagen) and Turbo DNase digestion (Invitrogen). RNA concentrations were
622 measured with a UV/VIS Spectrophotometer and visualized on a 2% agarose gel.
623
624 cDNA was generated from RNA using Superscript III reverse transcriptase (Thermo
625 Scientific). RT-qPCRs were performed using SYBR green master mix (Applied Biosystems) with
626 5ng of cDNA. Primers used to detect *recA* (VC0543), *cbb*$_3$ (VC1442), *bd*-I (VC1844), *bd*-II
627 (VCA0872), and *bd*-III (VC1571) are listed in S4 Table. Relative quantification of oxidase
628 expression was internally normalized to *recA* as the gene of reference and reported as relative
629 fold change to *bd-III* oxidase expression in anaerobic conditions which served as the
630 comparator target for analysis. Fold change was calculated using an elongated Pfaffl method for
631 gene expression analysis, which is described in detail in Supplemental Materials [65].
632

633 ## Infant Mouse Colonization Assays

634 Infant mice were infected as described previously [66]. Briefly, three- to five-day-old
635 mouse neonates (Charles River, Wilmington, MA) were orogastrically infected with
636 approximately 10^6 bacterial cells following 2 hours of separation from dam mice and maintained
637 at 30°C for 20h. After 20h, mice were euthanized, and intestinal segments weighed and
638 homogenized in 4ml phosphate buffered saline (PBS). Intestinal homogenates were serially
639 diluted and plated for CFU counts.
640

For single strain infections, dilutions were plated on LB streptomycin (100 µg/ml) for growth and enumeration. For MuGENT strain competition assays, dilutions were additionally plated on LB spectinomycin (200 µg/ml) for differentiation from co-infected wild type *V. cholerae.*

CoMPAS Infant Mouse Infection and Sequencing

Wild type, ^{Mu}*cbb*$_3$, ^{Mu}*bd*-I, ^{Mu}*bd*-II, and ^{Mu}*bd*-III MuGENT strains were combined in equal ratios and a total of 6 infant mice were infected with a final 0.01 OD_{600} inoculum, approximately ~10^6 CFU. Remaining inoculum volume was spun down at 4°C, 4000rpm, for 10min and DNA of the inoculum pool (IP) was isolated using a QIAamp PowerFecal Pro DNA Kit (Qiagen). After 20h infection, small intestinal segments were homogenized and pooled from the 6 infant mice. Pooled homogenates were filtered on ice using a 70µm filter to remove residual intestinal tissue. From here, DNA of the mouse pool (MP) was isolated using a QIAamp PowerFecal Pro DNA Kit (Qiagen).

Recovered DNA samples were normalized to 100ng/µl using Qubit dsDNA HS analysis and subsequently, multiplex amplicon sequencing was performed on both inoculum and mouse pools. Amplification targets included the primary subunit of each MuGENT oxidase complex (VC1442, VC1844, VCA0872, and VC1571) as well as *toxT* (VC0838) which is present in all input strains. Primers used are listed in S4 Table, amplification was carried out for 30 cycles. PCR products were purified using the QIAquick PCR Purification Kit (Qiagen) and quantified by Qubit dsDNA HS and normalized to 20ng/µl for MiSeq amplicon sequencing by the MSU RTSF Genomics Core (Michigan State University). Sequencing was conducted on a MiSeq Nano v2 flow cell using a 2x250bp paired end format. Sequence barcodes were trimmed and target loci read counts were quanitified using Geneious software.

In vitro Competition Assays

Bacterial strains were grown in 4ml LB media for 16-18h and resuspended to 1.0 OD_{600}. Wild type and an individual target strain were combined in a 1:1 ratio and used to inoculate deoxygenated LB for anaerobic competitions or benchtop LB for aerobic competitions. Anaerobic competitions were grown at 37°C static and aerobic competitions were grown 37°C 210rpm shaking. After 20h of growth, cultures were serially diluted and plated for colony forming units. WT vs. Aero7 and WT vs. Ana4 competitions were plated on LB streptomycin (100µg/ml), and LB spectinomycin (200µg/ml) to determine strain ratios. Individual deletion strain competitions were plated on LB streptomycin (100µg/ml) plus 5-bromo-4-chloro-3-indolyl β-D-galactopyranoside (X-Gal; 40µg/ml) for blue-white screening to determine strain ratios between a target strain and a Δ*lacZ* strain that served as a wild type comparison in the competition assays.

References

[1] Kaila VRI, Wikström M. Architecture of bacterial respiratory chains. Nat Rev Microbiol 2021;19:319–30. https://doi.org/10.1038/s41579-020-00486-4.

[2] Harris JB, LaRocque RC, Qadri F, Ryan ET, Calderwood SB. Cholera. Lancet, vol. 379, Lancet Publishing Group; 2012, p. 2466–76. https://doi.org/10.1016/S0140-6736(12)60436-X.

[3] Reen FJ, Almagro-Moreno S, Ussery D, Boyd EF. The genomic code: inferring Vibrionaceae niche specialization. Nat Rev Microbiol 2006;4:697–704. https://doi.org/10.1038/nrmicro1476.

[4] Bueno E, Sit B, Waldor MK, Cava F. Anaerobic nitrate reduction divergently governs population expansion of the enteropathogen Vibrio cholerae. Nat Microbiol 2018;3:1346–53. https://doi.org/10.1038/s41564-018-0253-0.

[5] Lee K-M, Park Y, Bari W, Yoon MY, Go J, Kim SC, et al. Activation of cholera toxin production by anaerobic respiration of trimethylamine N-oxide in Vibrio cholerae. J Biol Chem 2012;287:39742–52. https://doi.org/10.1074/jbc.M112.394932.

[6] Van Alst AJ, DiRita VJ. Aerobic metabolism in Vibrio cholerae is required for population expansion during infection. MBio 2020;11:1–15. https://doi.org/10.1128/mBio.01989-20.

[7] Bueno E, Sit B, Waldor MK, Cava F. Genetic dissection of the fermentative and respiratory contributions supporting Vibrio cholerae hypoxic growth. J Bacteriol 2020;202. https://doi.org/10.1128/JB.00243-20.

[8] Zheng L, Kelly CJ, Colgan SP. Physiologic hypoxia and oxygen homeostasis in the healthy intestine. A review in the theme: Cellular responses to hypoxia. Am J Physiol - Cell Physiol 2015;309:C350–60. https://doi.org/10.1152/ajpcell.00191.2015.

[9] Heidelberg JF, Eisen JA, Nelson WC, Clayton RA, Gwinn ML, Dodson RJ, et al. DNA sequence of both chromosomes of the cholera pathogen Vibrio cholerae. Nature

2000;406:477–83.

[10] Bueno E, Pinedo V, Cava F. Adaptation of Vibrio cholerae to hypoxic environments. Front Microbiol 2020;11:739. https://doi.org/10.3389/fmicb.2020.00739.

[11] Hemp J, Christian C, Barquera B, Gennis RB, Martínez TJ. Helix switching of a key active-site residue in the cytochrome cbb3 oxidases. Biochemistry 2005;44:10766–75. https://doi.org/10.1021/bi050464f.

[12] Ahn YO, Lee HJ, Kaluka D, Yeh SR, Rousseau DL, Ädelroth P, et al. The two transmembrane helices of CcoP are sufficient for assembly of the cbb3-type heme-copper oxygen reductase from Vibrio cholerae. Biochim Biophys Acta - Bioenerg 2015;1847:1231–9. https://doi.org/10.1016/j.bbabio.2015.06.013.

[13] Borisov VB, Gennis RB, Hemp J, Verkhovsky MI. The cytochrome bd respiratory oxygen reductases. Biochim Biophys Acta 2011:1398–413. https://doi.org/10.1016/j.bbabio.2011.06.016.

[14] Durand A, Bourbon ML, Steunou AS, Khalfaoui-Hassani B, Legrand C, Legrand A, et al. Biogenesis of the bacterial cbb3 cytochrome c oxidase: Active subcomplexes support a sequential assembly model. J Biol Chem 2018;293:808–18. https://doi.org/10.1074/jbc.M117.805184.

[15] Preisig O, Zufferey R, Thöny-Meyer L, Appleby CA, Hennecke H. A high-affinity cbb3-type cytochrome oxidase terminates the symbiosis-specific respiratory chain of Bradyrhizobium japonicum. J Bacteriol 1996;178:1532–8. https://doi.org/10.1128/jb.178.6.1532-1538.1996.

[16] Rice CW, Hempfling WP. Oxygen limited continuous culture and respiratory energy conservation in Escherichia coli. J Bacteriol 1978;134:115–24. https://doi.org/10.1128/jb.134.1.115-124.1978.

[17] Cotter PA, Melville SB, Albrecht JA, Gunsalus RP. Aerobic regulation of cytochrome d oxidase (cydAB) operon expression in Escherichia coli: roles of Fnr and ArcA in

repression and activation. Mol Microbiol 1997;25:605–15. https://doi.org/10.1046/j.1365-2958.1997.5031860.x.

[18] Smith A, Hill S, Anthony C. The purification, characterization and role of the d-type cytochrome oxidase of Klebsiella pneumoniae during nitrogen fixation. J Gen Microbiol 1990;136:171–80. https://doi.org/10.1099/00221287-136-1-171.

[19] Hughes ER, Winter MG, Duerkop BA, Spiga L, Furtado de Carvalho T, Zhu W, et al. Microbial respiration and formate oxidation as metabolic signatures of inflammation-associated dysbiosis. Cell Host Microbe 2017;21:208–19. https://doi.org/10.1016/j.chom.2017.01.005.

[20] Chanin RB, Winter MG, Spiga L, Hughes ER, Zhu W, Taylor SJ, et al. Epithelial-derived reactive oxygen species enable AppBCX-mediated aerobic respiration of Escherichia coli during intestinal inflammation. Cell Host Microbe 2020;28. https://doi.org/10.1016/j.chom.2020.09.005.

[21] Pitcher RS, Watmough NJ. The bacterial cytochrome cbb3 oxidases. Biochim Biophys Acta - Bioenerg 2004;1655:388–99. https://doi.org/10.1016/j.bbabio.2003.09.017.

[22] Jones SA, Gibson T, Maltby RC, Chowdhury FZ, Stewart V, Cohen PS, et al. Anaerobic respiration of Escherichia coli in the mouse intestine. Infect Immun 2011;79:4218–26. https://doi.org/10.1128/IAI.05395-11.

[23] Ito T, Gallegos R, Matano LM, Butler NL, Hantman N, Kaili M, et al. Genetic and biochemical analysis of anaerobic respiration in Bacteroides fragilis and its importance in vivo. MBio 2020;11. https://doi.org/10.1128/mBio.03238-19.

[24] Oh YT, Park Y, Yoon MY, Bari W, Go J, Min KB, et al. Cholera toxin production during anaerobic trimethylamine N-oxide respiration is mediated by stringent response in Vibrio cholerae. J Biol Chem 2014;289:13232–42. https://doi.org/10.1074/jbc.M113.540088.

[25] Dalia TN, Yoon SH, Galli E, Barre F-X, Waters CM, Dalia AB. Enhancing multiplex genome editing by natural transformation (MuGENT) via inactivation of ssDNA

exonucleases. Nucleic Acids Res 2017;45:7527–37. https://doi.org/10.1093/nar/gkx496.

[26] Skorupski K, Taylor RK. Positive selection vectors for allelic exchange. Gene 1996;169:47–52. https://doi.org/10.1016/0378-1119(95)00793-8.

[27] Dalia AB, Mcdonough E, Camilli A. Multiplex genome editing by natural transformation. Proc Natl Acad Sci U S A 2014;111:8937–42. https://doi.org/10.1073/pnas.1406478111.

[28] Ahn YO, Albertsson I, Gennis RB, Ädelroth P. Mechanism of proton transfer through the KC proton pathway in the Vibrio cholerae cbb3 terminal oxidase. Biochim Biophys Acta - Bioenerg 2018;1859:1191–8. https://doi.org/10.1016/j.bbabio.2018.08.002.

[29] Hayes CA, Dalia TN, Dalia AB. Systematic genetic dissection of PTS in *Vibrio cholerae* uncovers a novel glucose transporter and a limited role for PTS during infection of a mammalian host. Mol Microbiol 2017;104:568–79. https://doi.org/10.1111/mmi.13646.

[30] Thöny-Meyer L. Biogenesis of respiratory cytochromes in bacteria. Microbiol Mol Biol Rev 1997;61:337–76. https://doi.org/10.1128/mmbr.61.3.337-376.1997.

[31] Xia D, Esser L, Tang WK, Zhou F, Zhou Y, Yu L, et al. Structural analysis of cytochrome bc1 complexes: Implications to the mechanism of function. Biochim Biophys Acta - Bioenerg 2013;1827:1278–94. https://doi.org/10.1016/j.bbabio.2012.11.008.

[32] Blomberg MRA. The mechanism for oxygen reduction in the C family cbb3 cytochrome c oxidases - Implications for the proton pumping stoichiometry. J Inorg Biochem 2020;203:110866. https://doi.org/10.1016/j.jinorgbio.2019.110866.

[33] Jasaitis A, Borisov VB, Belevich NP, Morgan JE, Konstantinov AA, Verkhovsky MI. Electrogenic reactions of cytochrome bd. Biochemistry 2000;39:13800–9. https://doi.org/10.1021/bi001165n.

[34] Corbett D, Goldrick M, Fernandes VE, Davidge K, Poole RK, Andrew PW, et al. Listeria monocytogenes has both cytochrome bd-type and cytochrome aa 3 -type terminal oxidases, which allow growth at different oxygen levels, and both are important in infection. Infect Immun 2017;85:e00354-17. https://doi.org/10.1128/IAI.00354-17.

782 [35] Tseng CP, Albrecht J, Gunsalus RP. Effect of microaerophilic cell growth conditions on
783 expression of the aerobic (cyoABCDE and cydAB) and anaerobic (narGHJI, frdABCD,
784 and dmsABC) respiratory pathway genes in Escherichia coli. J Bacteriol 1996;178:1094–
785 8. https://doi.org/10.1128/jb.178.4.1094-1098.1996.
786 [36] Rivera-Chávez F, Zhang LF, Faber F, Lopez CA, Byndloss MX, Olsan EE, et al.
787 Depletion of butyrate-producing Clostridia from the gut microbiota drives an aerobic
788 luminal expansion of Salmonella. Cell Host Microbe 2016;19:443–54.
789 https://doi.org/10.1016/j.chom.2016.03.004.
790 [37] Arai H, Kawakami T, Osamura T, Hirai T, Sakai Y, Ishii M. Enzymatic characterization
791 and in vivo function of five terminal oxidases in Pseudomonas aeruginosa. J Bacteriol
792 2014;196:4206. https://doi.org/10.1128/JB.02176-14.
793 [38] Smith M, Finel M, Korolik V, Mendz G. Characteristics of the aerobic respiratory chains of
794 the microaerophiles Campylobacter jejuni and Helicobacter pylori. Arch Microbiol
795 2000;174:1–10. https://doi.org/10.1007/S002030000174.
796 [39] Hammer ND, Reniere ML, Cassat JE, Zhang Y, Hirsch AO, Hood MI, et al. Two heme-
797 dependent terminal oxidases power Staphylococcus aureus organ-specific colonization of
798 the vertebrate host. MBio 2013;4. https://doi.org/10.1128/mBio.00241-13.
799 [40] Spees AM, Wangdi T, Lopez CA, Kingsbury DD, Xavier MN, Winter SE, et al.
800 Streptomycin-induced inflammation enhances Escherichia coli gut colonization through
801 nitrate respiration. MBio 2013;4:430–43. https://doi.org/10.1128/MBIO.00430-13.
802 [41] Fu Y, Waldor MK, Mekalanos JJ. Tn-seq analysis of vibrio cholerae intestinal colonization
803 reveals a role for T6SS-mediated antibacterial activity in the host. Cell Host Microbe
804 2013;14:652–63. https://doi.org/10.1016/j.chom.2013.11.001.
805 [42] Borisov VB, Forte E, Davletshin A, Mastronicola D, Sarti P, Giuffrè A. Cytochrome bd
806 oxidase from Escherichia coli displays high catalase activity: An additional defense
807 against oxidative stress. FEBS Lett 2013;587:2214–8.

https://doi.org/10.1016/j.febslet.2013.05.047.

[43] Tardu M, Bulut S, Kavakli IH. MerR and ChrR mediate blue light induced photo-oxidative stress response at the transcriptional level in Vibrio cholerae. Sci Rep 2017;7. https://doi.org/10.1038/srep40817.

[44] Arjona D, Wikström M, Ädelroth P. Nitric oxide is a potent inhibitor of the *cbb* $_3$ -type heme-copper oxidases. FEBS Lett 2015;589:1214–8. https://doi.org/10.1016/j.febslet.2015.03.033.

[45] Jiménez de Bagüés MP, Loisel-Meyer S, Liautard J-P, Jubier-Maurin V. Different roles of the two high-oxygen-affinity terminal oxidases of Brucella suis: cytochrome c oxidase, but not ubiquinol oxidase, is required for persistence in mice. Infect Immun 2007;75:531–5. https://doi.org/10.1128/IAI.01185-06.

[46] Jünemann S. Cytochrome bd terminal oxidase. Biochim Biophys Acta - Bioenerg 1997;1321:107–27. https://doi.org/10.1016/S0005-2728(97)00046-7.

[47] Rivera-Chávez F, Mekalanos JJ. Cholera toxin promotes pathogen acquisition of host-derived nutrients. Nature 2019;572:244–8. https://doi.org/10.1038/s41586-019-1453-3.

[48] David LA, Weil A, Ryan ET, Calderwood SB, Harris JB, Chowdhury F, et al. Gut microbial succession follows acute secretory diarrhea in humans. MBio 2015;6:1–14. https://doi.org/10.1128/MBIO.00381-15.

[49] Ghosh P, Sinha R, Samanta P, Saha DR, Koley H, Dutta S, et al. Haitian variant Vibrio cholerae O1 strains manifest higher virulence in animal models. Front Microbiol 2019;10:110. https://doi.org/10.3389/fmicb.2019.00111.

[50] Liu Z, Wang H, Zhou Z, Naseer N, Xiang F, Kan B, et al. Differential thiol-based switches jump-start Vibrio cholerae pathogenesis. Cell Rep 2016;14:347–54. https://doi.org/10.1016/J.CELREP.2015.12.038.

[51] Malpica R, Franco B, Rodriguez C, Kwon O, Georgellis D. Identification of a quinone-sensitive redox switch in the ArcB sensor kinase. Proc Natl Acad Sci U S A

2004;101:13318–23. https://doi.org/10.1073/pnas.0403064101.

[52] Sengupta N, Paul K, Chowdhury R. The global regulator ArcA modulates expression of virulence factors in Vibrio cholerae. Infect Immun 2003;71:5583–9.

[53] Krishnan HH, Ghosh A, Paul K, Chowdhury R. Effect of anaerobiosis on expression of virulence factors in Vibrio cholerae. Infect Immun 2004;72:3961–7. https://doi.org/10.1128/IAI.72.7.3961-3967.2004.

[54] Murphy SG, Johnson BA, Ledoux CM, Dörr T. Vibrio cholerae's mysterious Seventh Pandemic island (VSP-II) encodes novel Zur-regulated zinc starvation genes involved in chemotaxis and cell congregation. PLOS Genet 2021;17:e1009624. https://doi.org/10.1371/JOURNAL.PGEN.1009624.

[55] Boin MA, Häse CC. Characterization of Vibrio cholerae aerotaxis. FEMS Microbiol Lett 2007;276:193–201. https://doi.org/10.1111/j.1574-6968.2007.00931.x.

[56] Butler SM, Camilli A. Both chemotaxis and net motility greatly influence the infectivity of Vibrio cholerae. Proc Natl Acad Sci U S A 2004;101:5018–23. https://doi.org/10.1073/pnas.0308052101.

[57] Jones SA, Chowdhury FZ, Fabich AJ, Anderson A, Schreiner DM, House AL, et al. Respiration of Escherichia coli in the mouse intestine. Infect Immun 2007;75:4891–9. https://doi.org/10.1128/IAI.00484-07.

[58] Sellars MJ, Hall SJ, Kelly DJ. Growth of Campylobacter jejuni supported by respiration of fumarate, nitrate, nitrite, trimethylamine-N-oxide, or dimethyl sulfoxide requires oxygen. J Bacteriol 2002;184:4187–96. https://doi.org/10.1128/JB.184.15.4187-4196.2002.

[59] Zeng MY, Inohara N, Nuñez G. Mechanisms of inflammation-driven bacterial dysbiosis in the gut. Mucosal Immunol 2017;10:18–26. https://doi.org/10.1038/mi.2016.75.

[60] Mamantopoulos M, Frising UC, Asaoka T, van Loo G, Lamkanfi M, Wullaert A. El Tor Biotype Vibrio cholerae activates the caspase-11-independent canonical Nlrp3 and pyrin inflammasomes. Front Immunol 2019;10:2463.

https://doi.org/10.3389/FIMMU.2019.02463.

[61] Klose KE. The suckling mouse model of cholera. Trends Microbiol 2000;8:189–91. https://doi.org/10.1016/S0966-842X(00)01721-2.

[62] Nygren E, Li BL, Holmgren J, Attridge SR. Establishment of an adult mouse model for direct evaluation of the efficacy of vaccines against Vibrio cholerae. Infect Immun 2009;77:3475–84. https://doi.org/10.1128/IAI.01197-08.

[63] Chong CYL, Bloomfield FH, O'Sullivan JM. Factors affecting gastrointestinal microbiome development in neonates. Nutrients 2018;10. https://doi.org/10.3390/NU10030274.

[64] Kelly CJ, Zheng L, Campbell EL, Saeedi B, Scholz CC, Bayless AJ, et al. Crosstalk between microbiota-derived short-chain fatty acids and intestinal epithelial HIF augments tissue barrier function. Cell Host Microbe 2015;17:662–71. https://doi.org/10.1016/j.chom.2015.03.005.

[65] Pfaffl MW. A new mathematical model for relative quantification in real-time RT–PCR. Nucleic Acids Res 2001;29:e45. https://doi.org/10.1093/NAR/29.9.E45.

[66] Anthouard R, DiRita VJ. Small-molecule inhibitors of toxT expression in Vibrio cholerae. MBio 2013;4:e00403-13. https://doi.org/10.1128/mBio.00403-13.

Supporting Information

Supplemental Methods

S1 Fig. MuGENT spectinomycin selective marker shows no fitness defect *in vitro*. Comparison of wild type and *ΔlacZ* C6706 *V. cholerae* strains with and without MuGENT spectinomycin selective marker in pseudogene VC1807. (a) Aerobic i*n vitro* competition assay after 20h. (b) Aerobic growth curve assay. (c) Anaerobic *in vitro* competition assay after 20h. (d) Anaerobic growth curve assay. All assays were performed in LB media. Bars in *in vitro* competitions represent the arithmetic mean where error bars represent the standard error of the mean. Growth curves are an average of three biological replicates where error bars represent the standard error of the mean.

S2 Fig. *cbb*$_3$ deficient strains and wild type grown anaerobically do not maintain a functional *cbb*$_3$ oxidase complex. *V. cholerae* cultures were grown on LB agar plates and spotted onto a rapid test DrySlide containing $N_1N_1N'_1N'$-tetramethyl-*p*-phenylene-diamine dihydrochloride (Wurster's blue; TMPD) that turns blue when reduced by cytochrome c oxidases. (a) *V. cholerae cbb*$_3$ mutant strain spots and *E. coli* (cytochrome c deficient) control. (b) Wild type *V. cholerae* grown in aerobic, microaerobic, and anaerobic conditions.

S3 Fig. *V. cholerae* oxidases generally support the same pattern of growth in minimal M9 0.2% D-glucose media as seen in LB and combinatorial MuGENT mutants closely recapitulate triple isogenic deletion mutant growth in LB. (a-b) Single terminal oxidase deletion mutants grown in M9 0.2% D-glucose, aerobically and anaerobically, respectively. Inoculums for all growth experiments were prepared in anaerobic conditions. (c-d) Combinatorial terminal oxidase deletion mutant growth in LB. Inoculums were prepared

anaerobically and subsequently grown in aerobic and anaerobic conditions, respectively. Triple deletion mutant strains have a '+' with an oxidase name (e.g. +*cbb*$_3$), indicating the sole remaining oxidase, with the other three oxidases disrupted by mutation. Growth curves are an average of three biological replicates where error bars represent the standard error of the mean.

S4 Fig. Terminal reductase mutants are variable for aerobic growth in the presence of cognate electron acceptor molecules. *V. cholerae* terminal reductase aerobic growth characteristics in LB in the presence and absence of alternative electron acceptors (a) 50mM fumarate, (b) 50mM trimethylamine-N-oxide (TMAO), (c) 50mM nitrate, and (d) 50mM dimethyl sulfoxide (DMSO). Inoculums were prepared aerobically. Closed symbols indicate LB growth media lacked an alternative electron acceptor whereas open symbols indicate LB growth media was supplemented with a given alternative electron acceptor. Growth curves are an average of three biological replicates where error bars represent the standard error of the mean.

S5 Fig. Functional terminal oxidases, but not alternative terminal reductases, are required for optimal colonization of the large intestine. Aero7 and Ana4 colonization of the large intestine in both single strain and competition infections. (a) Single strain infection of strain Aero7. (b) Competition infection of strain Aero7. (c) Single strain infection of strain Ana4. (d) Competition infection of strain Ana4. Bars represent the geometric mean. Horizontal dashed lines indicate the limit of detection (LOD) and red dots indicate recovered CFUs were below the LOD. Competitive index scores were calculated as [($Mutant_{Output}/WT_{Output}$) / ($Mutant_{Input}/WT_{Input}$)]. Statistical analysis was performed using GraphPad PRISM. *, $P < 0.05$. A Mann-Whitney U-test was used in the determination of significance between WT and Aero7. A Student's *t* test was performed on log transformed data in the determination of significance between WT and Ana4. Single strain *in vivo* colonization assays in the large intestine for (e) individual and (f) combinatorial oxidase deletion strains. (g) Single strain colonization of aerobically prepared wild

type and +*cbb*$_3$ oxidase inoculums in the large intestine. Triple deletion mutant strains have a '+' with an oxidase name (e.g. +*cbb*$_3$), indicating the sole remaining oxidase, with the other three oxidases disrupted by mutation. Bars represent the geometric mean. Horizontal dashed lines indicate LOD, and red dots indicate recovered CFUs were below the LOD. Statistical analysis was performed using GraphPad PRISM. *, $P < 0.05$. A Mann-Whitney U-test was used in the determination of significance between WT and Aero7 and WT and +*bd*-III whereas an Analysis of Variance with *post hoc* Dunnett's multiple comparisons test was conducted on log transformed CFU/g intestine for all other strain comparisons.

S6 Fig. TcpA production is functional and hydrogen peroxide tolerance is equivalent among individual oxidase deletion mutants. (a) Western blot visualization of TcpA, a required virulence factor in *V. cholerae* pathogenesis, in both standard and anaerobic AKI conditions. (b) Densitometry analysis of TcpA production in standard AKI conditions. (c) Densitometry analysis of TcpP production in anaerobic AKI conditions. TcpA levels are displayed as relative to TcpA production in wild type cells. ImageJ was used to perform the densitometry analysis across three biological replicates. Horizontal bars represent the arithmetic mean where error bars represent the standard deviation of the mean. (d) Hydrogen peroxide minimum inhibitory concentration determination of individual oxidase deletion strains. Growth percentage was calculated as a function of optical density for test strains in various concentrations of H_2O_2 (0.15625mM, 0.3125mM, 0.625mM, 1.25mM, 2.5mM, 5mM, and 10mM) divided by the optical density for wild type *V. cholerae* grown in LB media without H_2O_2. All strains showed signs of growth reduction at 1.25mM H_2O_2 and were all entirely inhibited for growth at 2.5mM H_2O_2. Data points represent the arithmetic mean of three biological replicates with error bars representing the standard error of the mean.

954 **S7 Fig. Variant +*bd*-III strain (+*bd*-III^{V}) indicates that the *bd*-III oxidase, when expressed, is**
955 **capable of supporting aerobic respiration in *V. cholerae* and colonization of the infant**
956 **mouse.** (a) Wild type and +*bd*-III strain (Δ*cbb*$_3$ Δ*bd*-I Δ*bd*-II) *bd*-III expression. Expression was
957 determined for the primary subunit of the *bd*-III oxidase VC1571. Dots represent biological
958 replicates of relative *bd*-III expression between +*bd*-III and wild type strains. Bars represent
959 arithmetic mean with error bars representing the standard error of the mean. (b-c) Wild type and
960 +*bd*-III^{V} growth in LB. Inoculums were prepared aerobically and subsequently grown in aerobic
961 and anaerobic conditions, respectively. Data points represent the mean of triplicate growth
962 curves with error bars representing the standard error of the mean. (d) *In vitro* expression of
963 terminal oxidases in +*bd*-III^{V} strain. Expression was determined for the primary subunit of each
964 oxidase complex (VC1442, VC1844, VCA0872, VC1571). Bars represent the arithemtic mean
965 with error bars representing the standard error of the mean. (e) Single strain infection of +*bd*-III^{V}
966 in the small intestine. (f) Single strain infection of +*bd*-III^{V} in the large intestine. Bars in single
967 strain infections represent the geometric mean. Statistical analysis was performed using
968 GraphPad PRISM. *, $P < 0.05$. A Student's *t* test was performed on log transformed data in the
969 determination of significance between WT and +*bd*-III^{V} in both the small and large intestine.
970
971 **S1 Table. Whole genome sequencing single nucleotide polymorphism analysis**
972 **annotation.**
973
974 **S2 Table. CoMPAS sequencing reads.**
975
976 **S3 Table. Bacteria strain list.**
977
978 **S4 Table. Primer list.**

a

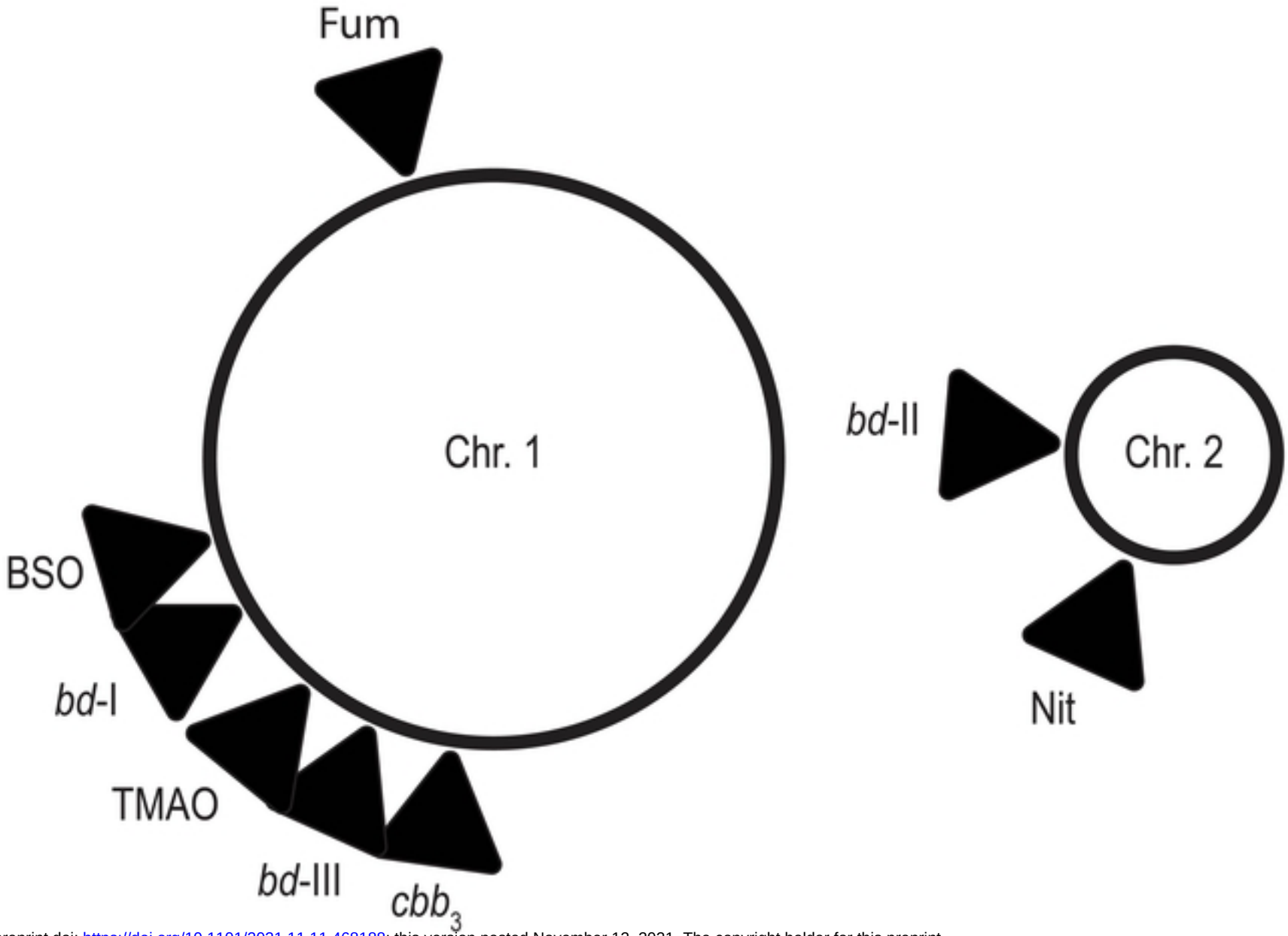

b

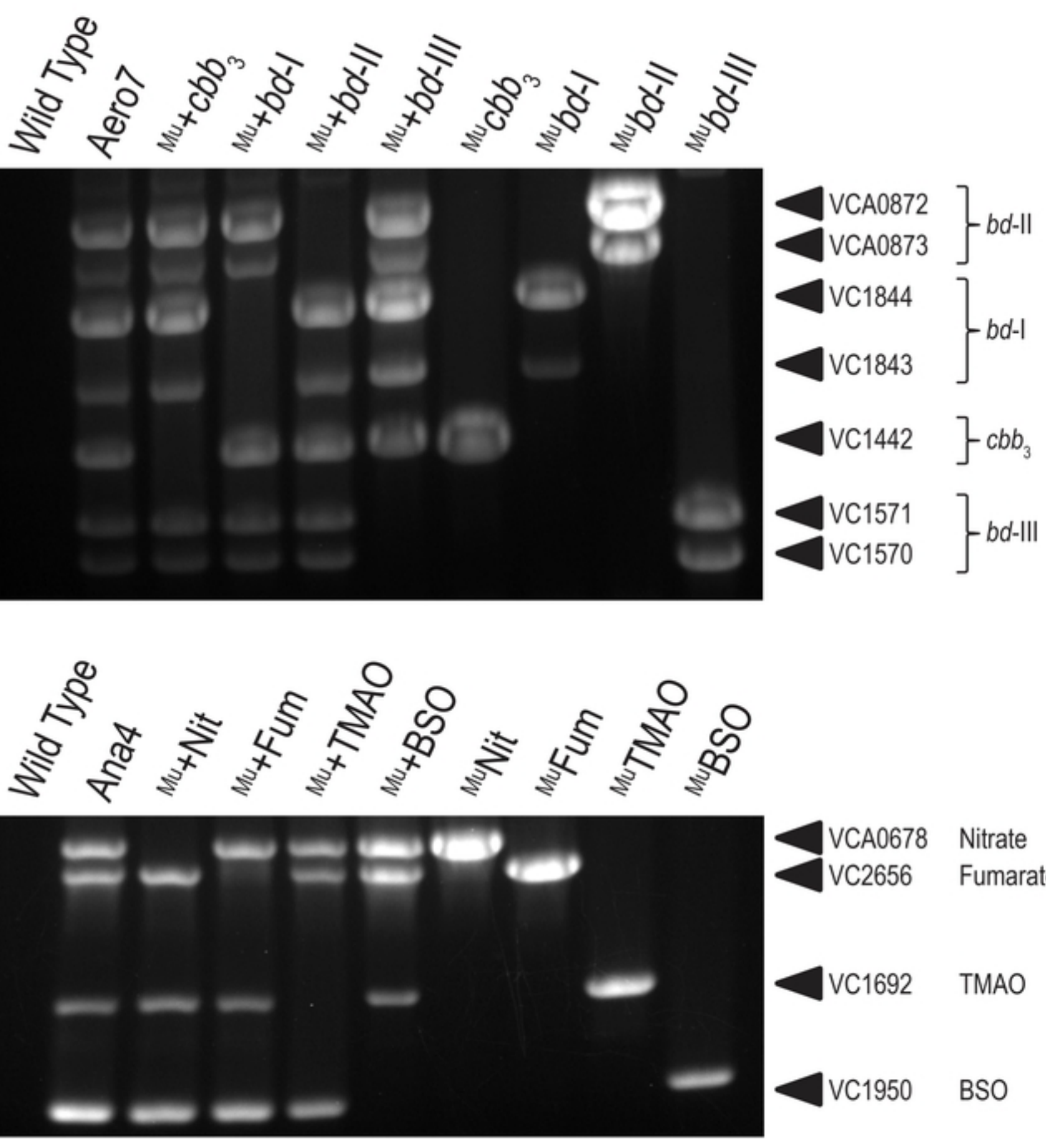

Figure 1

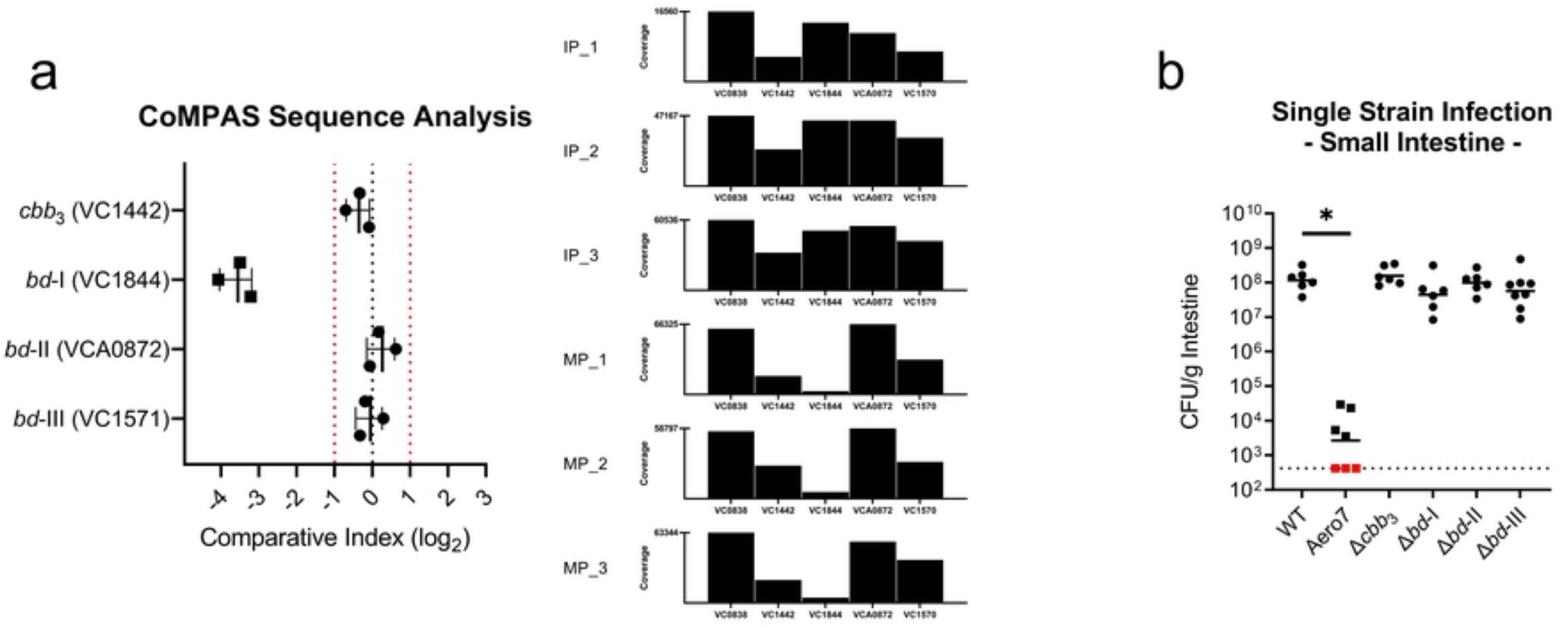
a
CoMPAS Sequence Analysis
cbb3 (VC1442)
bd-I (VC1844)
bd-II (VCA0872)
bd-III (VC1571)
-4
-3
-2
-1
0
1
2
3
Comparative Index (log2)
IP_1
IP_2
IP_3
MP_1
MP_2
MP_3
Coverage
VC0838
VC1442
VC1844
VCA0872
VC1570
b
Single Strain Infection
- Small Intestine -
CFU/g Intestine
*
WT
Aero7
Δcbb3
Δbd-I
Δbd-II
Δbd-III

Figure 6

a

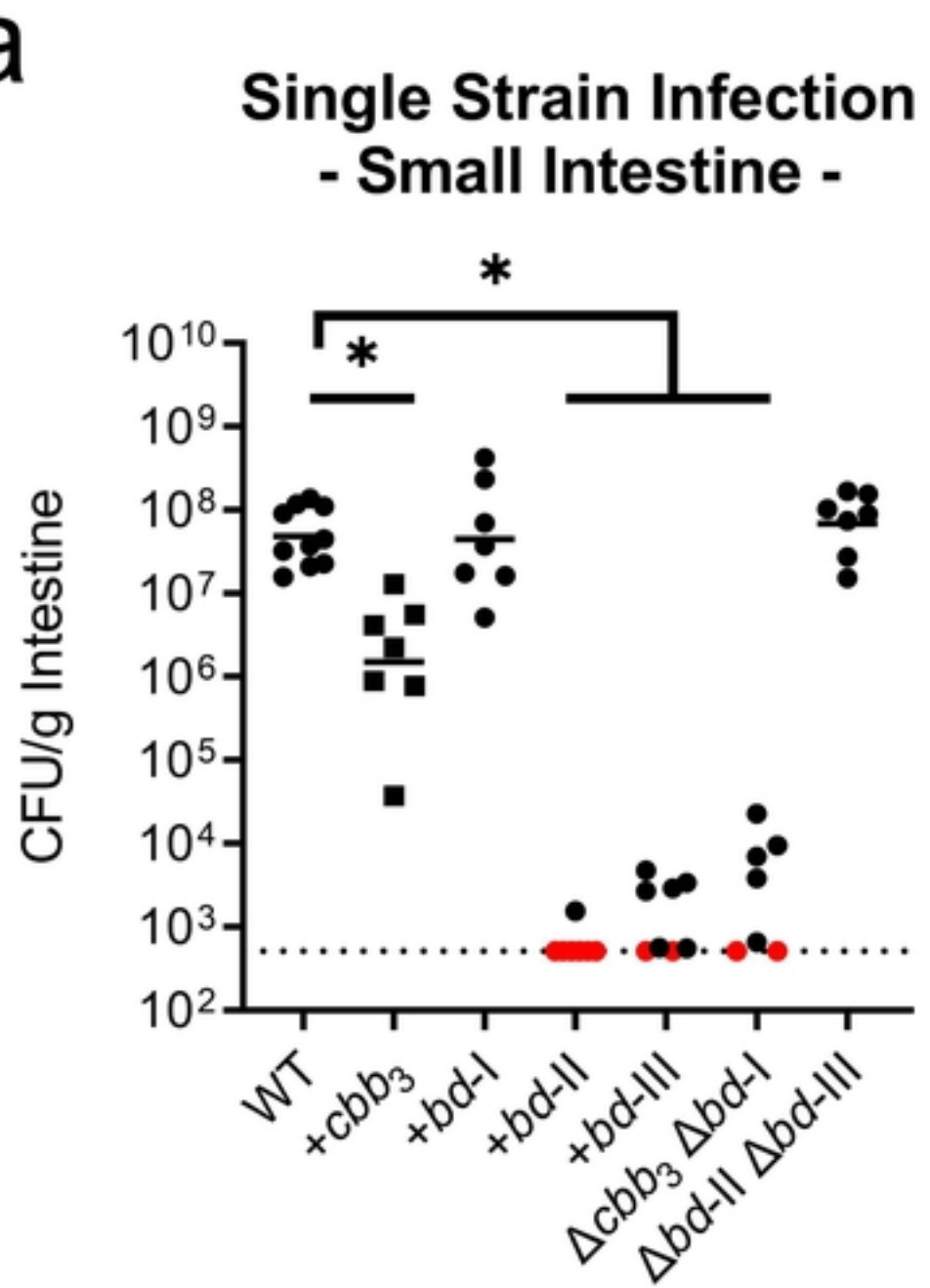
Single Strain Infection
- Small Intestine -
*
*
CFU/g Intestine
10^10
10^9
10^8
10^7
10^6
10^5
10^4
10^3
10^2
WT
+cbb3
+bd-I
+bd-II
+bd-III
Δcbb3 Δbd-I
Δbd-II Δbd-III

b

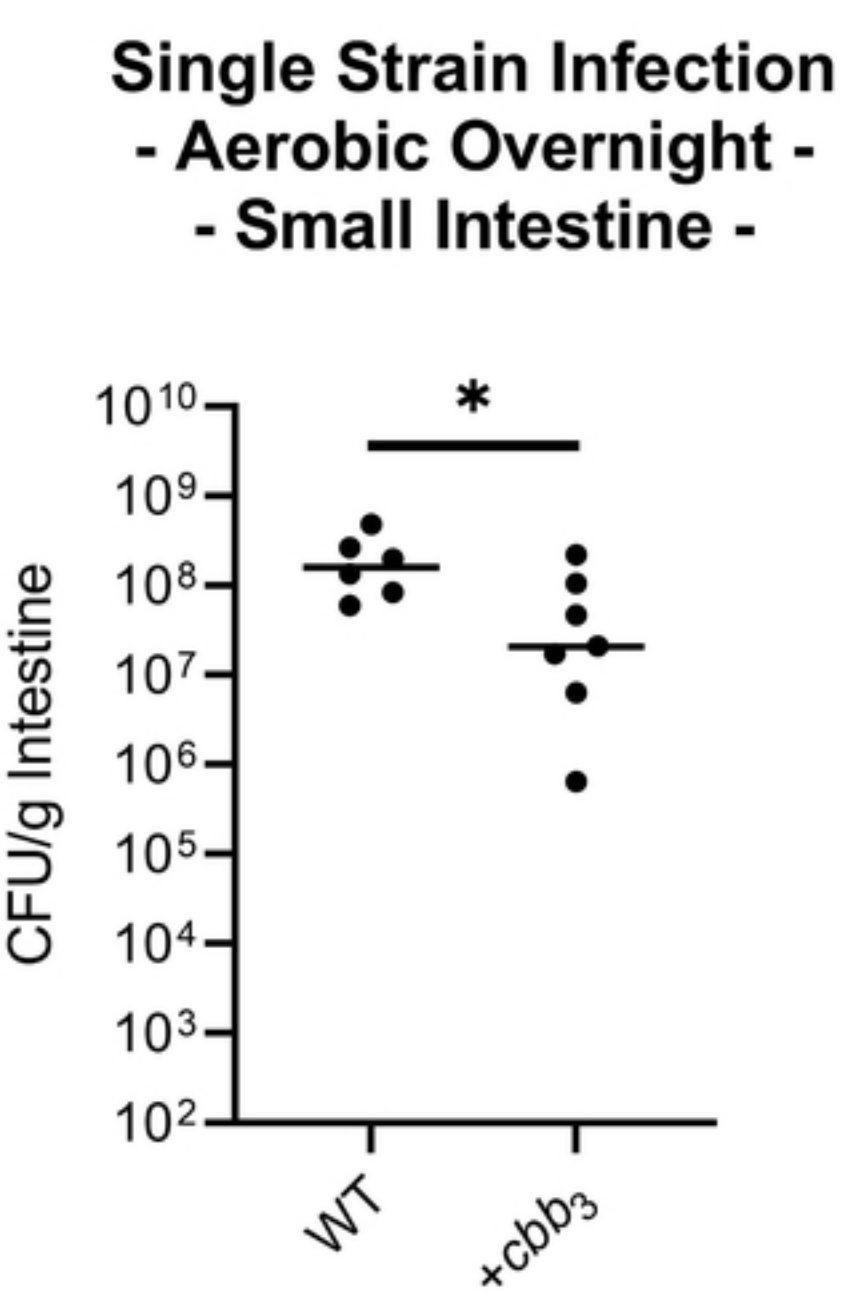
Single Strain Infection
- Aerobic Overnight -
- Small Intestine -
*
CFU/g Intestine
10^10
10^9
10^8
10^7
10^6
10^5
10^4
10^3
10^2
WT
+cbb3

Figure 7

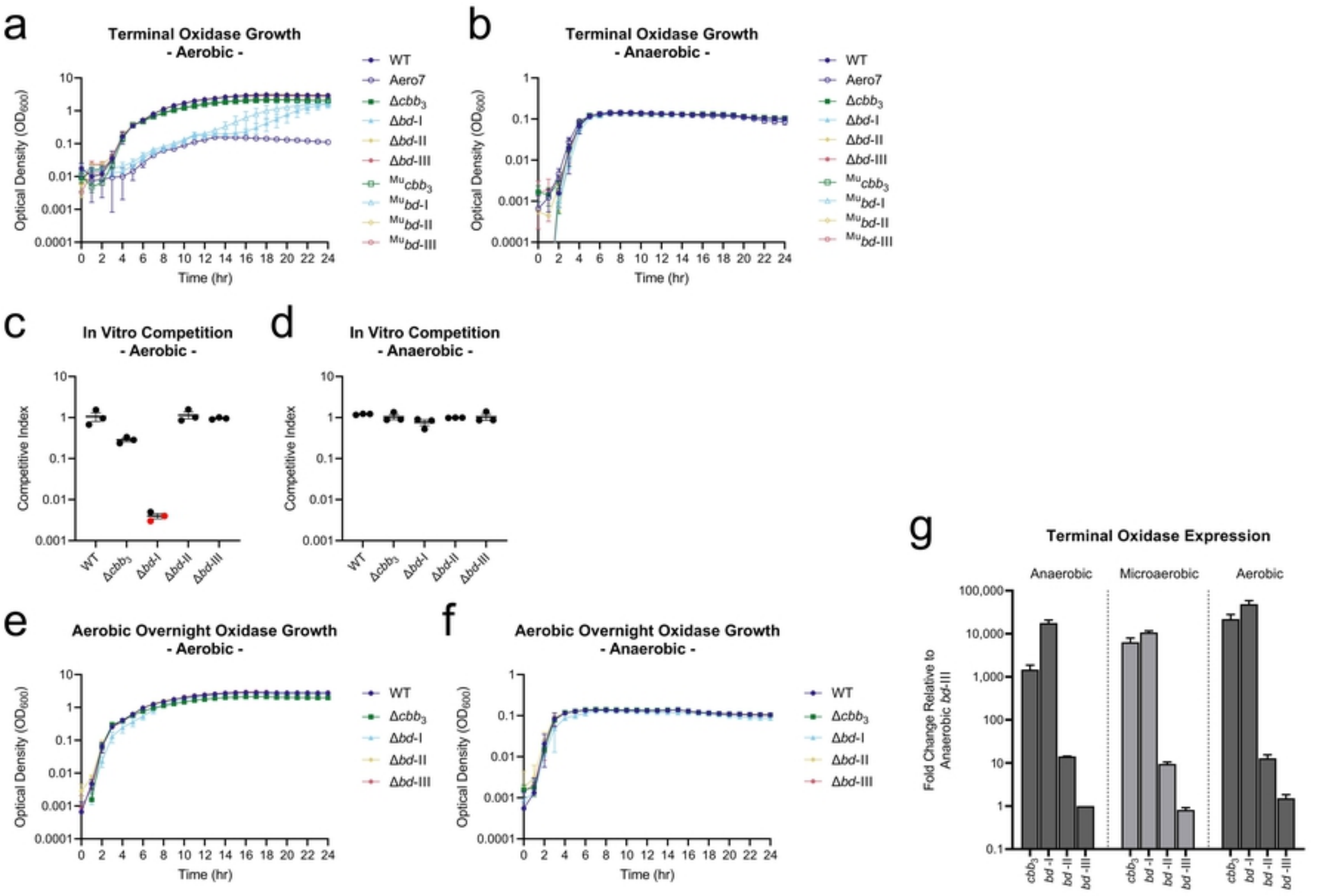
a
Terminal Oxidase Growth
- Aerobic -
Optical Density (OD600)
Time (hr)
WT
Aero7
Δcbb3
Δbd-I
Δbd-II
Δbd-III
Mucbb3
Mubd-I
Mubd-II
Mubd-III
b
Terminal Oxidase Growth
- Anaerobic -
Optical Density (OD600)
Time (hr)
WT
Aero7
Δcbb3
Δbd-I
Δbd-II
Δbd-III
Mucbb3
Mubd-I
Mubd-II
Mubd-III
c
In Vitro Competition
- Aerobic -
Competitive Index
WT
Δcbb3
Δbd-I
Δbd-II
Δbd-III
d
In Vitro Competition
- Anaerobic -
Competitive Index
WT
Δcbb3
Δbd-I
Δbd-II
Δbd-III
e
Aerobic Overnight Oxidase Growth
- Aerobic -
Optical Density (OD600)
Time (hr)
WT
Δcbb3
Δbd-I
Δbd-II
Δbd-III
f
Aerobic Overnight Oxidase Growth
- Anaerobic -
Optical Density (OD600)
Time (hr)
WT
Δcbb3
Δbd-I
Δbd-II
Δbd-III
g
Terminal Oxidase Expression
Anaerobic
Microaerobic
Aerobic
Fold Change Relative to Anaerobic bd-III
cbb3
bd -I
bd -II
bd -III

Figure 2

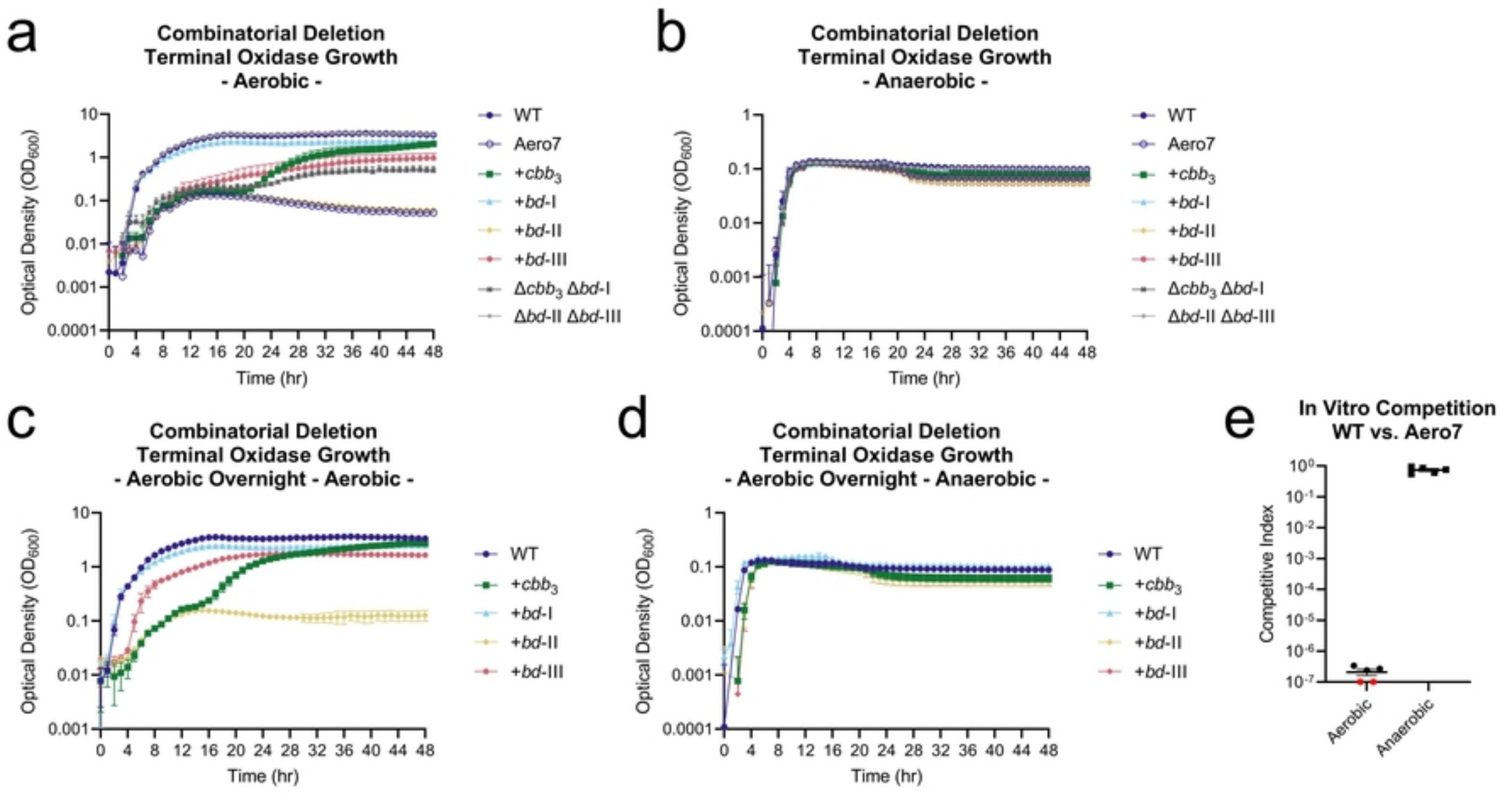
a
Combinatorial Deletion
Terminal Oxidase Growth
- Aerobic -
Optical Density (OD600)
Time (hr)
WT
Aero7
+cbb3
+bd-I
+bd-II
+bd-III
Δcbb3 Δbd-I
Δbd-II Δbd-III
b
Combinatorial Deletion
Terminal Oxidase Growth
- Anaerobic -
Optical Density (OD600)
Time (hr)
WT
Aero7
+cbb3
+bd-I
+bd-II
+bd-III
Δcbb3 Δbd-I
Δbd-II Δbd-III
c
Combinatorial Deletion
Terminal Oxidase Growth
- Aerobic Overnight - Aerobic -
Optical Density (OD600)
Time (hr)
WT
+cbb3
+bd-I
+bd-II
+bd-III
d
Combinatorial Deletion
Terminal Oxidase Growth
- Aerobic Overnight - Anaerobic -
Optical Density (OD600)
Time (hr)
WT
+cbb3
+bd-I
+bd-II
+bd-III
e
In Vitro Competition
WT vs. Aero7
Competitive Index
Aerobic
Anaerobic

Figure 3

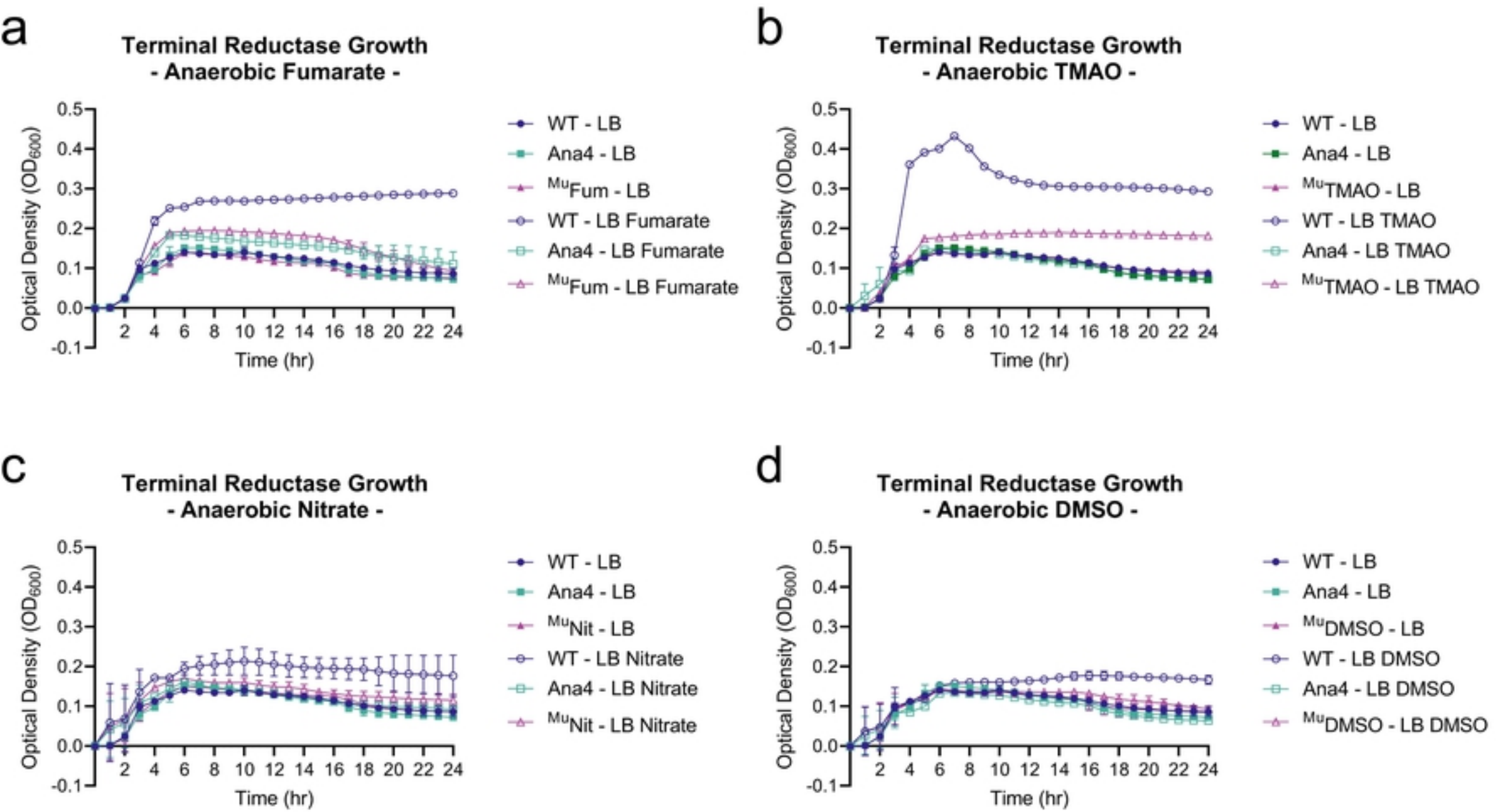
a
Terminal Reductase Growth
- Anaerobic Fumarate -
Optical Density (OD600)
Time (hr)
WT - LB
Ana4 - LB
MuFum - LB
WT - LB Fumarate
Ana4 - LB Fumarate
MuFum - LB Fumarate
b
Terminal Reductase Growth
- Anaerobic TMAO -
Optical Density (OD600)
Time (hr)
WT - LB
Ana4 - LB
MuTMAO - LB
WT - LB TMAO
Ana4 - LB TMAO
MuTMAO - LB TMAO
c
Terminal Reductase Growth
- Anaerobic Nitrate -
Optical Density (OD600)
Time (hr)
WT - LB
Ana4 - LB
MuNit - LB
WT - LB Nitrate
Ana4 - LB Nitrate
MuNit - LB Nitrate
d
Terminal Reductase Growth
- Anaerobic DMSO -
Optical Density (OD600)
Time (hr)
WT - LB
Ana4 - LB
MuDMSO - LB
WT - LB DMSO
Ana4 - LB DMSO
MuDMSO - LB DMSO

Figure 4

a

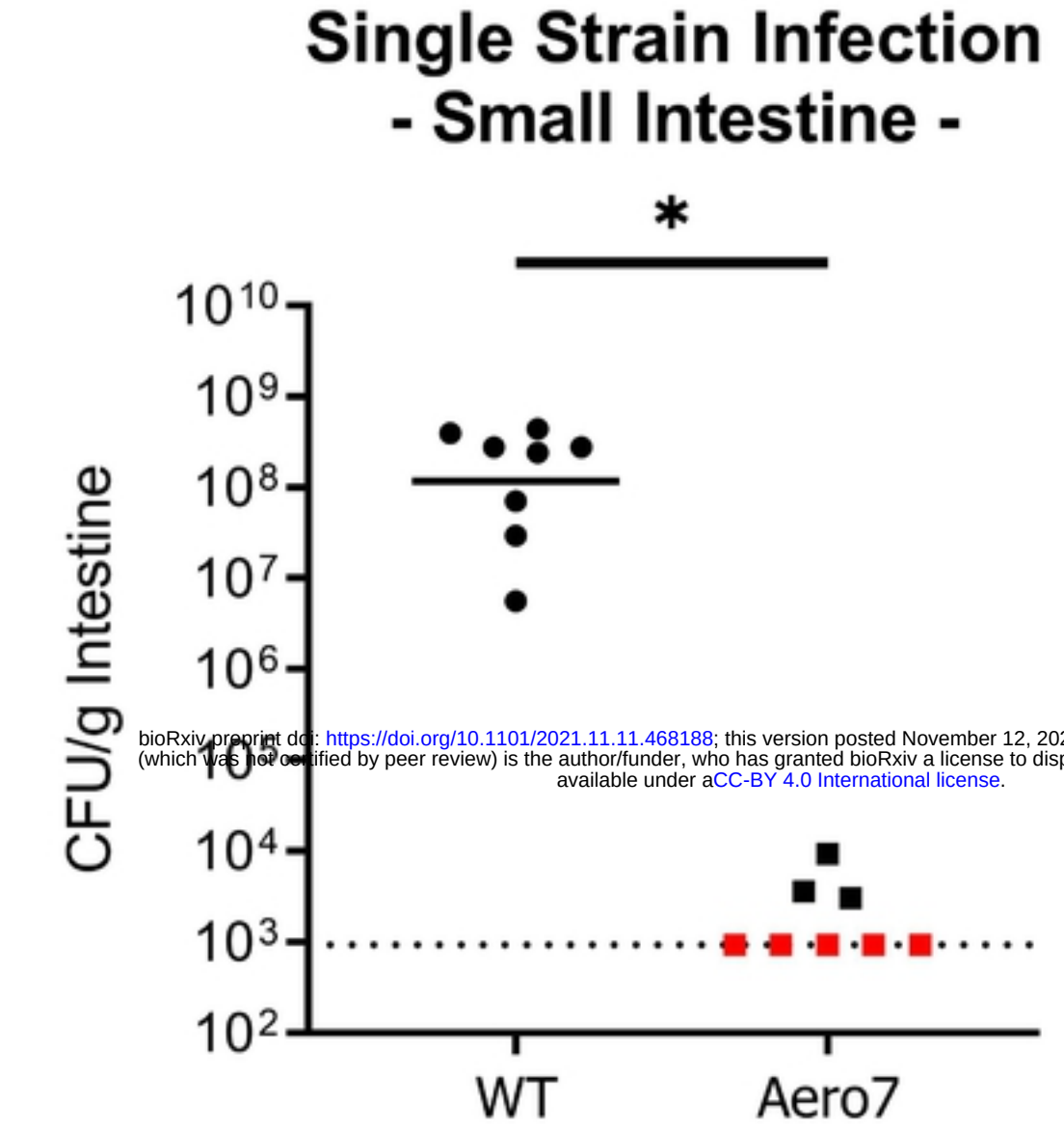

b

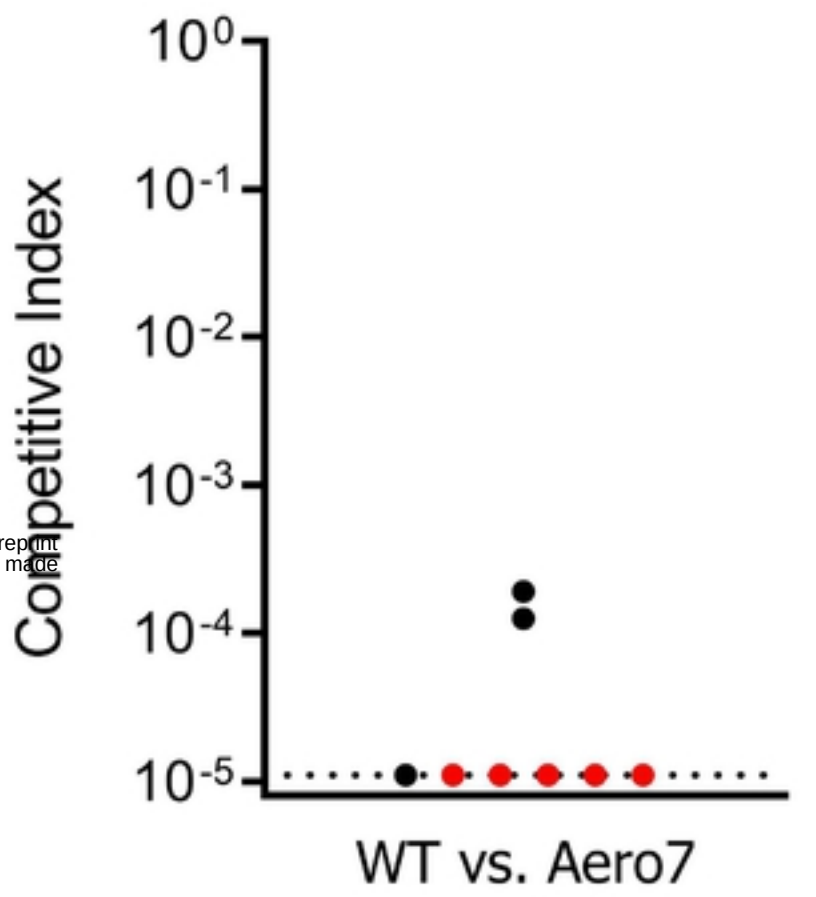

c

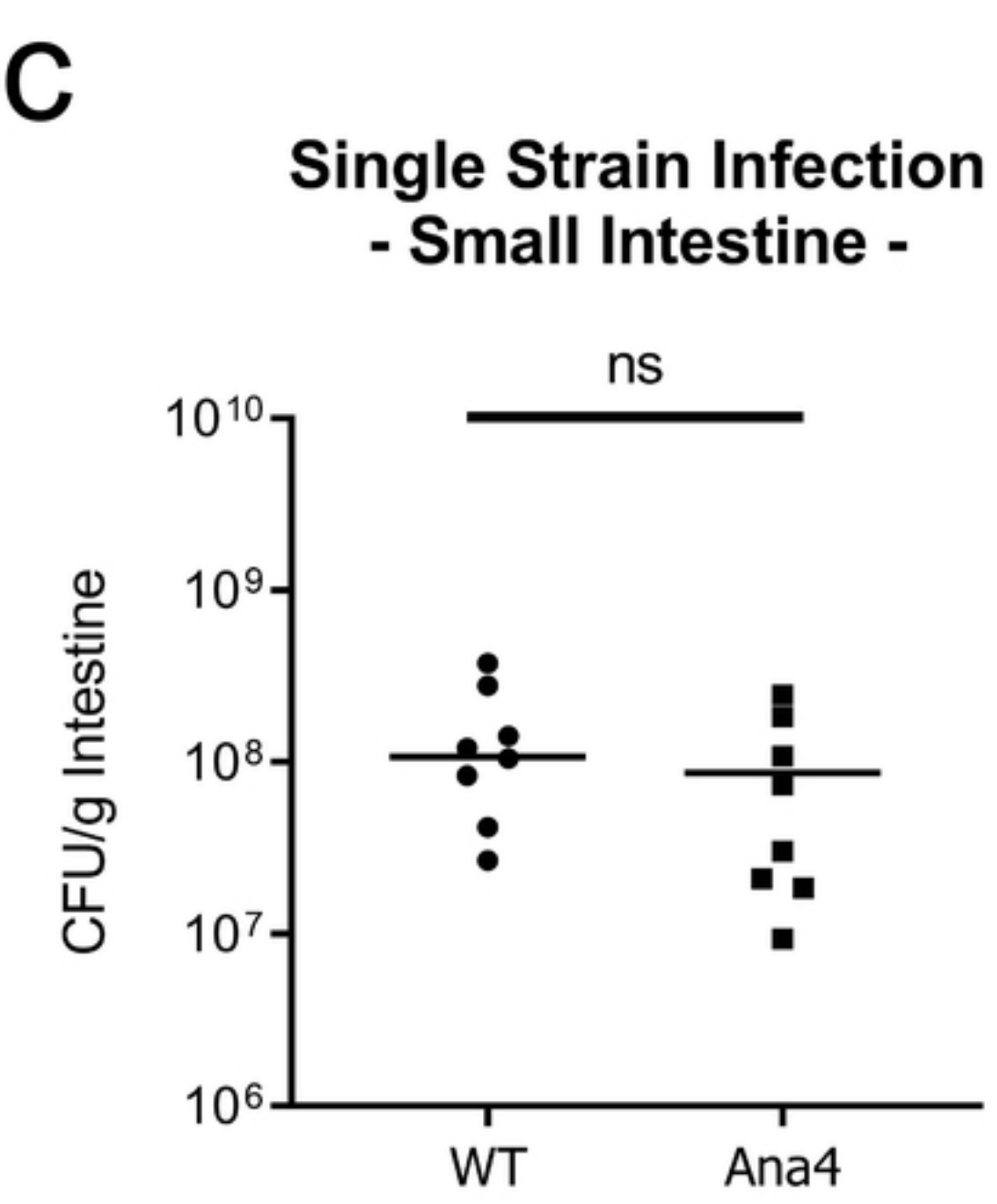

d

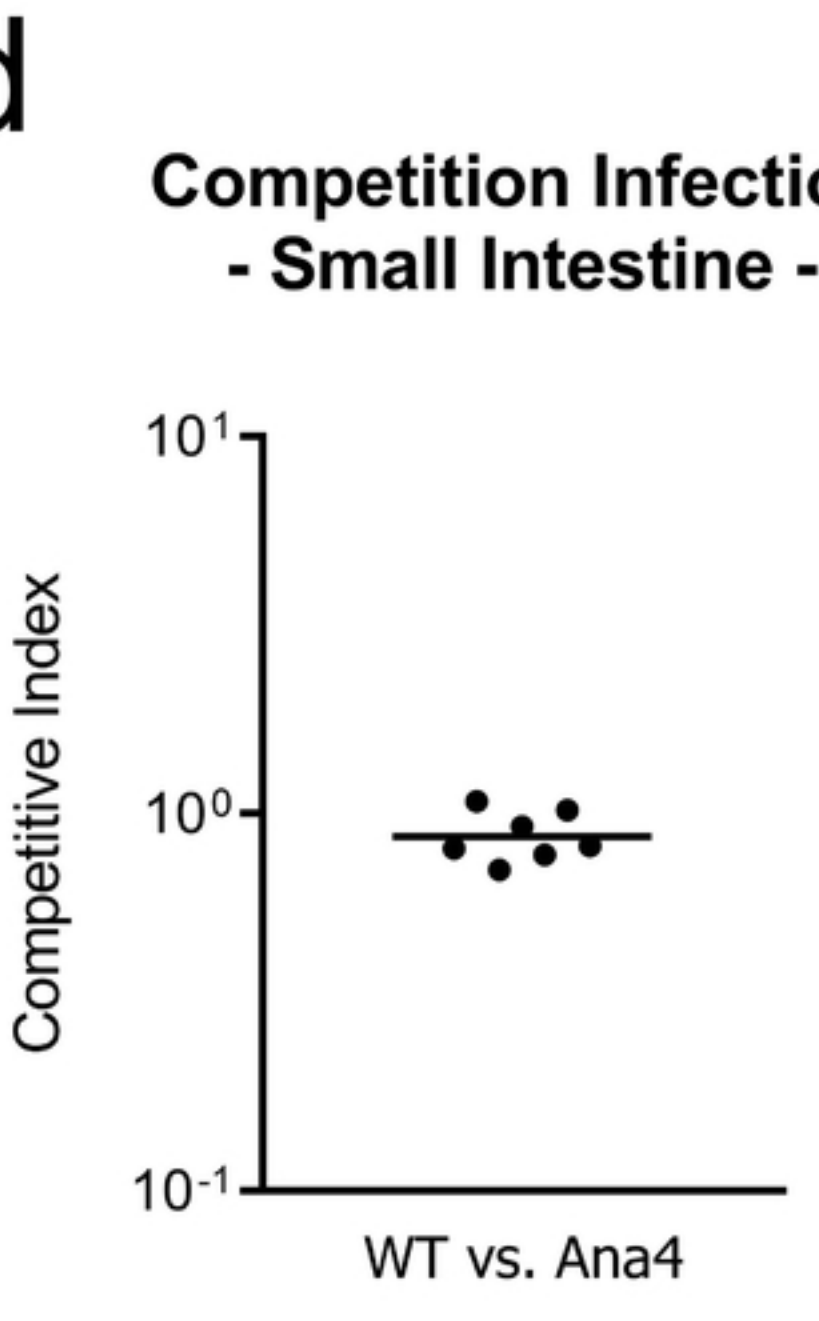

Figure 5